

Gibbs Sampling the Posterior of Neural Networks

Giovanni Piccioli,* Emanuele Troiani, and Lenka Zdeborová
École Polytechnique Fédérale de Lausanne (EPFL)
Statistical Physics of Computation Laboratory

In this paper, we study sampling from a posterior derived from a neural network. We propose a new probabilistic model consisting of adding noise at every pre- and post-activation in the network, arguing that the resulting posterior can be sampled using an efficient Gibbs sampler. The Gibbs sampler attains similar performances as the state-of-the-art Monte Carlo Markov chain methods, such as the Hamiltonian Monte Carlo or the Metropolis adjusted Langevin algorithm, both on real and synthetic data. By framing our analysis in the teacher-student setting, we introduce a thermalization criterion that allows us to detect when an algorithm, when run on data with synthetic labels, fails to sample from the posterior. The criterion is based on the fact that in the teacher-student setting we can initialize an algorithm directly at equilibrium.

I. INTRODUCTION

Neural networks are functions parametrized by the so-called weights, mapping inputs to outputs. Neural networks are commonly trained by seeking values of weights that minimize a prescribed loss function. In some contexts, however, we want to sample from an associated probability distribution of the weights. Such sampling is at the basis of Bayesian deep learning [50, 54]. It is used in Bayesian uncertainty estimation [25, 31, 46] or to evaluate Bayes-optimal performance in toy models where the data-generative process is postulated [3]. In this paper, we focus on studying the algorithms and properties of such sampling.

Given training inputs X in Bayesian learning, one implicitly assumes the labels to be generated according to the stochastic process $y \sim P(y|X, W)$, where W are the weight of the network, on which a prior $P(W|X)$ is placed. At its heart, Bayesian deep learning consists of sampling from the posterior probability of the parameters:

$$P(W|X, y) = \frac{P(y|W, X)P(W|X)}{P(y|X)}, \quad (1)$$

where we simply used Bayes theorem. This sampling problem is, in general, NP-hard [10], with many techniques being developed to sample from (1). In this paper, we look at iterative algorithms that in the large time limit, return samples from the posterior distribution (1). Most available algorithms for this task are based on MCMC methods. We focus on the two following questions:

- **Q1:** Do we have a method to evaluate whether the algorithms have thermalized, i.e., if the samples returned by the MCMC plausibly come from the posterior (1)?
- **Q2:** Which combinations of sampling algorithm and form of the posterior distribution achieve the best performance in terms of ability to thermalize while reaching a low test error?

The first question addresses the long-standing problem of estimating an MCMC’s thermalization time, that is, the time at which the MCMC starts sampling well from the posterior. We propose a criterion for thermalization based on the teacher-student setting. The criterion can only be reliably applied to synthetic labels generated by a teacher network. After a comparison with other thermalization heuristics, we argue that the teacher-student criterion is more discriminative, in that it provides a higher lower bound to the thermalization time. The second question explores the interplay between the form of the posterior and the sampling algorithm: since there is more than one way of translating a network architecture into a probabilistic process, we exploit this freedom to introduce a generative process in which noise is added at every pre- and post-activation of the network. We then design a Gibbs sampler tailored to this posterior and compare it to other commonly used MCMCs.

* giovannipiccioli@gmail.com

A. Related literature

When running an MCMC one has to wait a certain number of iterations for the algorithm to start sampling from the desired probability measure. We will refer to this burn-in period as the thermalization time or T_{therm} [41]. Samples before T_{therm} should therefore be discarded. Estimating T_{therm} is thus of great practical importance, as it is crucial to know how long the MCMC should be run. More formally, we initialize the MCMC with a δ -peaked distribution as its initial condition $P_{t=0}(x) = \delta_{x,x_0}$ where $x_0 \in \mathcal{X}$ is a starting state of our liking. Then, the probability from which the MCMC samples evolves according to $P_{t+1}(x) = \sum_{x' \in \mathcal{X}} P_t(x')P(x_{t+1} = x|x_t = x')$ [15], where the kernel $P(x_{t+1} = x'|x_t = x)$ contains the transition probabilities of the MCMC. If this kernel satisfies the detailed balance condition with respect to a probability $\pi(\cdot)$, and the chain is ergodic, then for $t \rightarrow \infty$, $P_t(x) \rightarrow \pi(x)$, and thus the MCMC will sample from π . In this setting, the thermalization time represents the time after which P_t is sufficiently close to π . The actual thermalisation threshold will change depending on the metric we use to measure the distance between P_t and π . Most commonly used distances between distributions P and Q can be written in the form $d(P, Q) = \sup_{\varphi \in \mathcal{F}} \{\sum_{x \in \mathcal{X}} \varphi(x)(P(x) - Q(x))\}$, with \mathcal{F} a function space that determines how strict the convergence is. One of the strictest metrics is the total variation distance d_{TV} , obtained by picking $\mathcal{F}_{TV} = \{\varphi : \varphi \text{ measurable, } \|\varphi\|_{\infty} \leq 1\}$. This distance gives rise to the definition of mixing time as the smallest t for which $d_{TV}(P_t, \pi) \leq 1/4$. Analytical bounds on the mixing time can be obtained using the transition kernel's spectral properties [27]. These results, however, are of difficult practical application, and the convergence metric might be too strict for practical purposes. A looser definition is that of weak convergence, which corresponds to a distance d_w given by $\mathcal{F}_w = \{\varphi \text{ s.t. } \|\varphi\|_{\infty} + \|\varphi\|_{Lip} \leq 1\}$ [48]. For $d_w(P_t, \pi)$ to be small, all Lipschitz bounded functions must have a similar expectation under P_t and π . This requirement can still be too strict: for example, in the statistical physics literature [41] [57] [34] one only includes in \mathcal{F} functions φ whose output concentrates in the thermodynamic limit, giving rise to d_{statphys} . We prefer to leave the definition of T_{therm} a bit vague since, from a practical point of view, none of the above convergence metrics can be so far computed efficiently.

Practitioners have instead resorted to a number of heuristics, which provide lower bounds to the thermalization time. These heuristics usually revolve around two ideas. We first have methods involving multiple chains [5, 9, 16, 41]. In different flavours, all these criteria rely on comparing multiple chains with different initializations. Once all the chains have thermalized, samples from different chains should be indistinguishable. Another approach consists of finding functions with known mean under the posterior and verifying whether the empirical mean is also close to its predicted value [9, 13, 19, 20, 58]. The proposed method for detecting thermalization relies instead on the teacher-student framework [57].

Another field we connect with is that of Bayesian learning of neural networks. For an introduction see [18, 24, 32, 50] and references therein. We shall first examine the probabilistic models for Bayesian learning of neural networks and then review the algorithms that are commonly used to sample. In order to specify the posterior (1), one needs to pick the likelihood (or data generating process) $P(y|X, W)$. The most common model, employed in the great majority of works [23, 39, 47, 52, 54] is $P(y|X, W) = \frac{1}{Z} \exp\left(-\frac{1}{2\Delta} \sum_{\mu} \ell(y^{\mu}, f(X^{\mu}, W))\right)$, where $f(\cdot, W)$ is the neural network function, ℓ is the loss function, μ is the sample index, and Δ is a temperature parameter. As an alternative, other works have introduced the "stochastic feedforward networks" (SFFN), where noise is added at every layer's pre-activation [37, 42, 45, 56]. Outside of the Bayesian learning of neural networks literature, models where intermediate pre- or post-activations are added as dynamical variables have also been considered in the predictive coding literature [2, 35, 36, 53].

Once a probabilistic model has been chosen, the goal is to obtain samples from the corresponding posterior. A first solution consists of approximating the posterior with a simpler distribution, which is easier to sample. This is the strategy followed by variational inference methods [26, 30, 31, 45, 49, 55]. Although variational inference yields fast algorithms, it is often based on uncontrolled approximations. Another category of approximate methods is that of "altered MCMCs", i.e., Monte Carlo algorithms which have been modified to be faster at the price of not sampling anymore from the posterior [7, 28, 29, 38, 40, 59]. An example of these algorithms is the discretized Langevin dynamics [51]. Restricting the sampling to a subset of the parameters has also been considered in [44] as an alternative training technique.

Finally, we have exact sampling methods: these are iterative algorithms that in the large time limit are guaranteed to return samples from the posterior distribution. Algorithms for exact sampling mostly rely on MCMC methods. The most popular ones are Hamiltonian Monte Carlo (HMC) [12, 39], Metropolis adjusted Langevin algorithm (MALA) [4, 33, 43] and the No U-turn sampler (NUTS)[22]. Within the field of Bayesian learning in neural networks, HMC is the most commonly used algorithm [23, 52, 54]. The proposed Gibbs sampler is inspired to the work of [1], and later [14, 21], that introduced the idea of augmenting the variable space in the context of logistic and multinomial regression.

II. TEACHER-STUDENT THERMALIZATION CRITERION

In this section we explain how to use the teacher-student setting to build a thermalization test for sampling algorithms. The test gives a lower bound on the thermalization time. We start by stating the main limitation of this approach: the criterion can only be applied to synthetic datasets. In other words, the training labels y must be generated by a teacher network, using the following procedure.

We first pick arbitrarily the training inputs and organize them into an $n \times d$ matrix X . Each row X^μ of the matrix is a different training sample, for a total of n samples. We then sample the teacher weights W_\star from the prior $P(W)$. Finally, we generate the noisy training labels as $y^\mu \sim P(y|X^\mu, W_\star)$. Our goal is to draw samples from the posterior $P(W|D)$, where $D = \{(X^\mu, y^\mu)\}_{\mu \in [n]}$ indicates the training set. Suppose we want to have a lower bound on the thermalization time of a MCMC initialized at a particular configuration W_{start} . The method consists of running two parallel chains $W_1(t)$ and $W_2(t)$. For the first chain, we use an informed initialization, meaning we initialize the chain on the teacher weights, thus setting $W_1(t=0) = W_\star$. For second chain we set $W_2(t=0) = W_{\text{start}}$. To determine convergence we consider a test function $g(W)$. We first run the informed initialization: after some time T_1 , $g(W_1(t))$ will become stationary. Using samples collected after T_1 we compute the expected value of g (let us call it \bar{g}). Next, we run the second chain. The lower bound to the thermalization time of $W_2(t)$ is the time where $g(W_2(t))$ becomes stationary and starts oscillating around \bar{g} . In practice, this time is determined by visually inspecting the time series of g under the two initializations, and observing when the two merge.

At first glance this method does not seem too different from [16] or [5], whose method (described in Appendix A) relies on multiple chains with different initializations. There is however a crucial difference: the informed initialization is already thermalized at $t=0$. To see this, recall that the pair W_\star, D was obtained by first sampling W_\star from $P(W)$ and then sampling D from $P(D|W_\star)$. This implies that W_\star, D is a sample from the joint distribution $P(W, D)$. Rewriting $P(W, D) = P(W|D)P(D)$, we see that W_\star is also typical under the posterior distribution. In conclusion, the power of the teacher-student setting lies in the fact that it gives us access to one sample from the posterior, namely W_\star . It then becomes easier to check whether a second chain is sampling from the posterior by comparing the value of a test function. In contrast, other methods comparing chains with different initialization have no guarantee that if the two chains "merge" then the MCMC is sampling from the posterior, since it is possible that both chains are trapped together far from equilibrium.

III. THE INTERMEDIATE NOISE MODEL

In this section, we introduce a new probabilistic model for Bayesian learning of neural networks. We start by reviewing the classical formulation of Bayesian learning of neural networks. Let $f(x, W)$ be the neural network function, with W its parameters, and $x \in \mathbb{R}^d$ the input vector. Given a training set $X \in \mathbb{R}^{n \times d}, y \in \mathbb{R}^n$ we aim to sample from

$$P(W|X, y) = \frac{1}{P(y|X)} P(W) \exp \left[-\frac{1}{2\Delta} \sum_{\mu=1}^n \ell(y^\mu, f(X^\mu, W)) \right], \quad (2)$$

where $\ell(\cdot, \cdot)$ is the single sample loss function, and Δ a temperature parameter. Notice that to derive (2) from (1), we supposed that $P(W|X) = P(W)$, i.e., W is independent of X . This is a common and widely adopted assumption in the Bayesian learning literature, and we shall make it in what follows. Most works in the field of Bayesian learning of neural networks attempt to sample from (2). This form of the posterior corresponds to the implicit assumption that the labels were generated by

$$y^\mu \sim P_{\text{out}}(y|f(X^\mu, W)), \text{ with } P_{\text{out}}(y|z) \propto e^{-\frac{1}{2\Delta} \ell(y, z)} \quad (3)$$

where W are some weights sampled from the prior. We propose an alternative generative model based on the idea of introducing a small Gaussian noise at every pre- and post-activation in the network. The motivation behind this process lies in the fact that we are able to sample the resulting posterior efficiently using a Gibbs sampling scheme. Consider the case where $f(\cdot, W)$ is a multilayer perceptron with L layers, without biases and with activation function $\sigma(\cdot)$. Hence we have $f(x, W) = W^{(L)} \sigma(W^{(L-1)} \sigma(\dots \sigma(W^{(1)} x) \dots))$. Here $W^{(\ell)} \in \mathbb{R}^{d_{\ell+1} \times d_\ell}$ indicates the weights of layer $\ell \in [L]$, with d_ℓ the width of the layer. We define the pre-activations $Z^{(\ell)} \in \mathbb{R}^{n \times d_\ell}$ and post activations

$X^{(\ell)} \in \mathbb{R}^{n \times d_\ell}$ of layer ℓ . Using Bayes theorem and applying the chain rule to the likelihood we obtain

$$\begin{aligned} P(\{X^{(\ell)}\}_{\ell=2}^L, \{Z^{(\ell)}\}_{\ell=2}^L, \{W^{(\ell)}\}_{\ell=1}^L | X, y) = \\ \frac{1}{P(y|X)} P(\{W^{(\ell)}\}_{\ell=1}^L) P(y, \{X^{(\ell)}\}_{\ell=2}^L, \{Z^{(\ell)}\}_{\ell=2}^L | \{W^{(\ell)}\}_{\ell=1}^L, X) = \frac{1}{P(y|X)} P(\{W^{(\ell)}\}_{\ell=1}^L) \times \\ \times \left[\prod_{\ell=2}^L P(Z^{(\ell+1)} | X^{(\ell)}, W^{(\ell)}) P(X^{(\ell)} | Z^{(\ell)}) \right] P(Z^{(2)} | X, W^{(1)}) \end{aligned} \quad (4)$$

with the constraint $Z^{(L+1)} = y$. The conditional probabilities are assumed to be

$$P(Z^{(\ell+1)} | X^{(\ell)}, W^{(\ell)}) = \prod_{\mu=1}^n \prod_{\alpha=1}^{d_{\ell+1}} \mathcal{N}\left(Z_{\alpha}^{(\ell+1)\mu} | W_{\alpha}^{(\ell)T} X^{(\ell)\mu}, \Delta_Z^{(\ell+1)}\right) \quad (5)$$

$$P(X^{(\ell)} | Z^{(\ell)}) = \prod_{\mu=1}^n \prod_{i=1}^{d_\ell} \mathcal{N}\left(X_{\alpha}^{(\ell)\mu} | \sigma(Z_i^{(\ell)\mu}), \Delta_X^{(\ell)}\right), \quad (6)$$

where $\{\Delta_Z^{(\ell)}\}_{\ell=2}^{L+1}$, $\{\Delta_X^{(\ell)}\}_{\ell=2}^L$ control the amount of noise added at each pre- and post- activation. This structure of the posterior implicitly assumes that the pre- and post-activations are iteratively generated as

$$Z^{(\ell+1)} = X^{(\ell)} W^{(\ell)T} + \epsilon_Z^{(\ell+1)}, \quad X^{(\ell+1)} = \sigma(Z^{(\ell+1)}) + \epsilon_X^{(\ell+1)}, \quad \ell \in [L]. \quad (7)$$

$X^{(1)} = X \in \mathbb{R}^{n \times d}$ are the inputs, $Z^{(L+1)} = y \in \mathbb{R}^n$ represent the labels and $\epsilon_Z^{(\ell)}, \epsilon_X^{(\ell)}$ are $n \times d_\ell$ matrices of i.i.d. respectively $\mathcal{N}(0, \Delta_Z^{(\ell)})$ and $\mathcal{N}(0, \Delta_X^{(\ell)})$ elements. We will refer to (7) as the intermediate noise generative process.

If we manage to sample from the posterior (4), which has been augmented with the variables $\{X^{(\ell)}\}_{\ell=2}^L, \{Z^{(\ell)}\}_{\ell=2}^L$, then we can draw samples from $P(W|X, y)$, just by discarding the additional variables. A drawback of this posterior is that one has to keep in memory all the pre- and post-activations in addition to the weights.

We remark that the intermediate noise generative process admits the classical generative process (3) and the SFNN generative model as special cases. Setting all Δ s (and hence all ϵ) to zero in (7) except for $\Delta_Z^{(L+1)}$ indeed gives back the classical generative process (3), with $\ell(y, z) = (y - z)^2$ and $\Delta = \Delta_Z^{(L+1)}$. Instead, setting $\Delta_X^{(\ell)} = 0$ for all ℓ , but keeping the noise in the pre-activations gives the SFNN model.

IV. GIBBS SAMPLER FOR NEURAL NETWORKS

Gibbs sampling [17] is an MCMC algorithm that updates each variable in sequence by sampling it from its conditional distribution. For a probability measure with three variables $P(\theta_1, \theta_2, \theta_3)$, one step of Gibbs sampling can be described as follows. Starting from the configuration $\theta_1(t), \theta_2(t), \theta_3(t)$, we first draw $\theta_1(t+1) \sim P(\theta_1 | \theta_2(t), \theta_3(t))$, then we draw $\theta_2(t+1) \sim P(\theta_2 | \theta_1(t+1), \theta_3(t))$ and finally $\theta_3(t+1) \sim P(\theta_3 | \theta_1(t+1), \theta_2(t+1))$. Repeating this procedure one can prove [6] that, in the limit of many iterations ($t \gg 1$) and provided that the chain is ergodic, the samples $(\theta_1(t), \theta_2(t), \theta_3(t))$ will come from $P(\theta_1, \theta_2, \theta_3)$. We now present a Gibbs sampler for the intermediate noise posterior (4), with Gaussian prior. More specifically the prior on $W^{(\ell)}$ is i.i.d. $\mathcal{N}(0, 1/\lambda_W^{(\ell)})$ over the weights' coordinates. The full derivation of the algorithm is reported in Appendix C, here we sketch the main steps. To define the sampler we need to compute the distributions of each of $X^{(\ell)}, Z^{(\ell)}, W^{(\ell)}$ conditioned on all other variables (here indicated by "All"). For $X^{(\ell)}$ the conditional distribution factorizes over samples $\mu \in [n]$, leading to

$$P(X^{(\ell)\mu} | \text{All}) = P(X^{(\ell)\mu} | Z^{(\ell)\mu}, W^{(\ell)}, Z^{(\ell+1)\mu}) = \mathcal{N}(X^{(\ell)\mu} | (m^{(X_\ell)})^\mu, \Sigma^{(X_\ell)}). \quad (8)$$

This is a multivariate Gaussian with covariance $\Sigma^{(X_\ell)} = \left(\frac{1}{\Delta_Z^{(\ell+1)}} W^{(\ell)T} W^{(\ell)} + \frac{1}{\Delta_X^{(\ell)}} \mathbb{1}_{d_\ell} \right)^{-1}$, and mean $(m^{(X_\ell)})^\mu = \Sigma^{(X_\ell)} \left(\frac{1}{\Delta_X^{(\ell)}} \sigma(Z^{(\ell)\mu}) + \frac{1}{\Delta_Z^{(\ell+1)}} W^{(\ell)T} Z^{(\ell+1)\mu} \right)$.

Considering $W^{(\ell)}$, we exploit that the conditional factorizes over the rows $\alpha \in [d_{\ell+1}]$.

$$P(W_{\alpha}^{(\ell)} | \text{All}) = P(W_{\alpha}^{(\ell)} | X^{(\ell)}, Z_{\alpha}^{(\ell+1)}) = \mathcal{N}(W_{\alpha}^{(\ell)} | (m_W^{(\ell)})_{\alpha}, \Sigma_W^{(\ell)}), \quad (9)$$

with $\Sigma_W^{(\ell)} = \left(\frac{1}{\Delta_Z^{(\ell+1)}} X^{(\ell)T} X^{(\ell)} + \lambda_W^{(\ell)} \mathbb{1}_{d_\ell} \right)^{-1}$, and $(m_W^{(\ell)})_{\alpha} = \frac{1}{\Delta_Z^{(\ell+1)}} \Sigma_W^{(\ell)} X^{(\ell)T} Z_{\alpha}^{(\ell+1)}$.

For $Z^{(\ell+1)}$ the conditional factorizes both over samples and over coordinates. We have

$$P(Z_\alpha^{(\ell+1)\mu} | \text{All}) = P(Z_\alpha^{(\ell+1)\mu} | X_\alpha^{(\ell+1)\mu}, W_\alpha^{(\ell)}, X^{(\ell)\mu}) \propto \exp \left[-\frac{1}{2\Delta_Z^{(\ell+1)}} \left(Z_\alpha^{(\ell+1)\mu} - W_\alpha^{(\ell)T} X^{(\ell)\mu} \right)^2 - \frac{1}{2\Delta_X^{(\ell+1)}} \left(\sigma(Z_\alpha^{(\ell+1)\mu}) - X_\alpha^{(\ell+1)\mu} \right)^2 \right]. \quad (10)$$

Notice that the conditional distributions of $W_\alpha^{(\ell)}$ and $X^{(\ell)\mu}$ are multivariate Gaussians and can be easily sampled. Instead $Z_\alpha^{(\ell)\mu}$ is a one-dimensional random variable with non Gaussian distribution. Appendix E provides recipes for sampling it for sign, ReLU and absolute value activations.

Algorithm 1 Gibbs sampler for MLP

Input: training inputs X , training labels y , noise variances $\{\Delta_Z^{(\ell)}\}_{\ell=2}^{L+1}$, $\{\Delta_X^{(\ell)}\}_{\ell=2}^L$, prior inverse variances $\{\lambda_W^{(\ell)}\}_{\ell=1}^L$, initial condition $\{X^{(\ell)}\}_{\ell=2}^L, \{W^{(\ell)}\}_{\ell=1}^L, \{Z^{(\ell)}\}_{\ell=2}^L$, length of the simulation t_{\max}
Output: a sequence S of samples
 $X^{(1)} \leftarrow X$
 $Z^{(L+1)} \leftarrow y$
 $S \leftarrow [(\{W^{(\ell)}\}_{\ell=1}^L, \{X^{(\ell)}\}_{\ell=2}^L, \{Z^{(\ell)}\}_{\ell=2}^L)]$
for $t = 1, \dots, t_{\max}$ **do**
 $W^{(1)} \sim P(W^{(1)} | X, Z^{(2)})$ ▷ See eq. (9)
for $\ell = 2, \dots, L$ **do**
 $X^{(\ell)} \sim P(X^{(\ell)} | Z^{(\ell)}, W^{(\ell)}, Z^{(\ell+1)})$ ▷ See eq. (8)
 $W^{(\ell)} \sim P(W^{(\ell)} | X^{(\ell)}, Z^{(\ell+1)})$ ▷ See eq. (9)
 $Z^{(\ell)} \sim P(Z^{(\ell)} | X^{(\ell-1)}, W^{(\ell-1)}, X^{(\ell)})$ ▷ See eq. (10)
end for
 $S.append(\left(\{W^{(\ell)}\}_{\ell=1}^L, \{X^{(\ell)}\}_{\ell=2}^L, \{Z^{(\ell)}\}_{\ell=2}^L\right))$
end for

Putting all ingredients together, we obtain the Gibbs sampling algorithm, whose pseudocode is reported in Algorithm 1. The main advantages of Gibbs sampling lie in the fact that it has no hyperparameters to tune and, moreover, it is a rejection-free sampling method. In the case of MCMCs, hyperparameters are defined to be all parameters that can be changed without affecting the probability measure that the MCMC asymptotically samples. The Gibbs sampler can also be parallelized across layers: a parallelized version of Algorithm 1 is presented in Appendix D. Finally, one can also extend this algorithm to more complex architectures: Appendices F and G contain respectively the update equations for biases and convolutional networks. We release an implementation of the Gibbs sampler at <https://github.com/SPOC-group/gibbs-sampler-neural-networks>.

V. NUMERICAL RESULTS

In this section we present numerical experiments to support our claims. We publish the code to reproduce these experiments at <https://github.com/SPOC-group/numerics-gibbs-sampling-neural-nets>.

A. Teacher student convergence method

In section II we proposed a thermalization criterion based on having access to an already thermalized initialization. Here we show that it is more discriminative than other commonly used heuristics. We first briefly describe these heuristics.

- **Stationarity.** Thermalization implies stationarity since once the MCMC has thermalized, it samples from a fixed probability measure. Therefore any observable, plotted as a function of time should oscillate around a constant value. The converse (stationarity implies thermalization) is not true. Nevertheless observing when a function becomes stationary gives a lower bound on T_{therm} .

- **Score method** [13]. Given a probability measure $P(x)$, we exploit the fact that $\mathbb{E}_{x \sim P} \left[\frac{\partial \log P(x)}{\partial x} \right] = \int \frac{\partial P(x)}{\partial x} dx = 0$.

We then monitor the function $\frac{\partial \log P(x)}{\partial x}$ along the dynamics. The time at which it starts fluctuating around zero is another lower bound to T_{therm} .

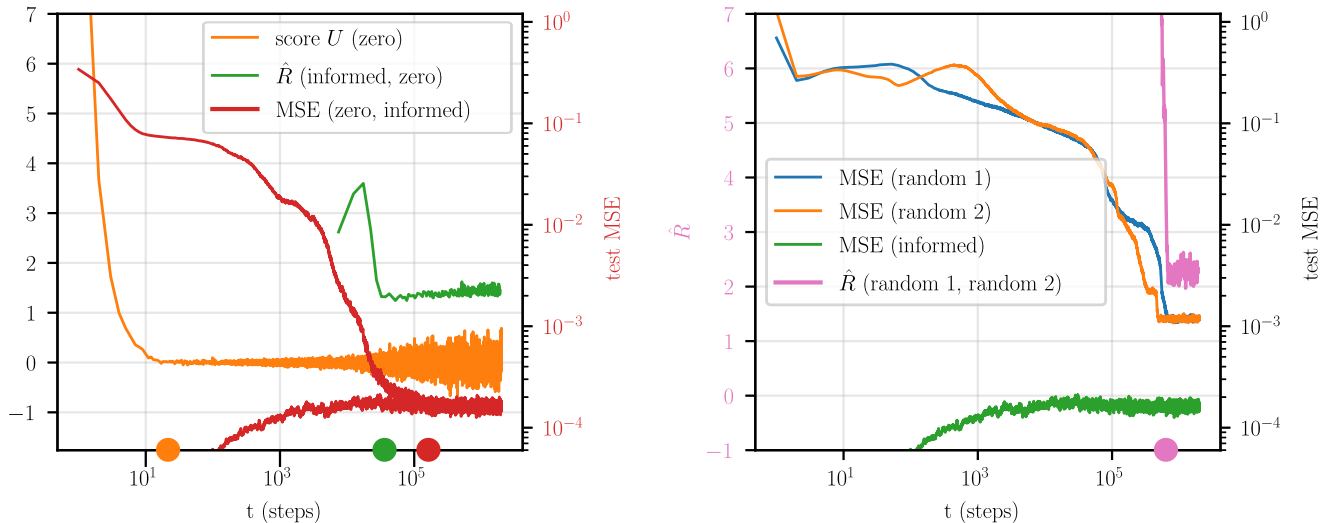


FIG. 1. Comparison of different thermalization measures. In the legend, next to each method we write between parentheses the initialization (or pair of initializations) the method is applied to. The circles on the x axis represent the thermalization times estimated by each method. **Left:** We compare the predictions for the thermalization time of the zero-initialized MCMC. The red y scale on the right refers uniquely to the lines in red. All the other quantities should be read on the black y scale. **Right:** We compare the predictions for the thermalization time of two chains initialized independently at random. The pink y scale refers uniquely to the pink line. All other quantities should be read on the black logarithmic scale. The randomly initialized runs fail to thermalize and their test MSEs get stuck on a plateau. However, \hat{R} , whose time series on the plateau is stationary and close to 1, fails to detect this lack of thermalization.

- **\hat{R} statistic** [16]. Two (or more) MCMCs are run in parallel starting from different initializations. The within-chain variance is compared to the total variance, obtained by merging samples from both chains. Call the ratio of these variances \hat{R} (a precise definition of which is given in Appendix A). If the MCMC has thermalized, the samples from the two chains should be indistinguishable, thus \hat{R} will be close to 1. The time at which \hat{R} gets close to 1 provides yet another lower bound to the thermalization time.

We compare these methods in the case of a one hidden layer neural network, identical for the teacher and the student, with input dimension $d_1 = 50$, $d_2 = 10$ hidden units and a scalar output. This corresponds to the function

$$f(x, W) = b^{(2)} + W^{(2)}\sigma\left(W^{(1)}x + b^{(1)}\right), \quad (11)$$

where $\sigma(x) = \max(0, x)$ and W indicates the collection of all parameters: $W^{(1)} \in \mathbb{R}^{d_2 \times d_1}$ and $W^{(2)} \in \mathbb{R}^{1 \times d_2}$. We specify the prior by setting $\lambda_W^{(1)} = \lambda_b^{(1)} = d_1$, $\lambda_W^{(2)} = \lambda_b^{(2)} = d_2$, the prior on the bias $b^{(\ell)}$ is $\mathcal{N}(0, 1/\lambda_b^{(\ell)})$ i.i.d. over the coordinates of the bias vector. Let $n = 2084$ be the size of the training set. We pick n to be four times the number of parameters in the network anticipating that the training set contains enough information to learn the teacher. We start by generating the matrix of training inputs $X \in \mathbb{R}^{n \times d_1}$ with i.i.d. standard Gaussian entries, then we sample the teacher's weights W_\star from the Gaussian prior. For concreteness we set $\Delta_Z^{(2)}, \Delta_X^{(2)}, \Delta_Z^{(3)}$ to the same value Δ and set $\Delta = 10^{-4}$. To generate the training labels y , we feed X , the teacher's weights W_\star and Δ into the generative process (7), adapted to also add the biases. For the test set, we first sample X_{test} , with i.i.d. standard Gaussian entries. Both the test labels and the test predictions are generated in a noiseless way (i.e., just passing the inputs through the network). In this way, the test error takes the following form: $\text{test MSE} = \frac{1}{n_{\text{test}}} \sum_{\mu=1}^{n_{\text{test}}} (f(X_{\text{test}}^\mu, W_\star) - f(X_{\text{test}}^\mu, W))^2$. The full details about this experiment set are in Appendix B. We run the Gibbs sampler on the intermediate noise posterior starting from three different initializations: informed, zero and random. Respectively the student's variables are initialized to the teacher's counterparts, to zero, or are sampled from the prior. In this particular setting, the Gibbs sampler initialized at zero manages to thermalize, while the random initializations fail to do so. Two independent random initializations are shown, in order to be able to use the multiple chains method.

Figure 1 illustrates a representative result of these experiments. In the left panel, we aim to find the highest lower bound to the thermalization time of the zero-initialized chain. Looking at the score method we plot $U = \Delta \frac{1}{d_1 d_2} \sum_{i=1}^{d_1} \sum_{\alpha=1}^{d_2} \frac{\partial \log P}{\partial W_{\alpha i}^{(1)}}$, where P indicates the posterior distribution; this is the score rescaled by Δ and averaged

over the first layer weights. In the zero-initialized chain, U starts oscillating around zero already at $t = 20$. Then we consider the \hat{R} statistics computed on the outputs of the two chains with zero and informed initializations. The criterion estimates that the zero-initialized chain has thermalized after $t = 6 \times 10^4$, when \hat{R} approaches 1 and becomes stationary. Next, we consider the teacher-student method, with the test MSE as the test function (g in our previous discussion). According to this method, the MCMC thermalizes after the test MSE time series of the informed and zero-initialized chains merge, which happens around $t = 10^5$. Finally, the stationarity criterion, when applied to the test MSE or to \hat{R} gives a similar estimate for the thermalization time. The x -axis of the left plot provides a summary of this phenomenology, by placing a circle at the thermalization time estimated by each method. In summary, the teacher-student method is the most conservative, but the \hat{R} statistics-based method is also reasonable here.

The right panel of Fig. 1 then shows a representative situation where thermalization is not reached yet the \hat{R} statistics-based method would indicate it is. In the right panel, two randomly initialized chains, denoted by *random 1* and *random 2* are considered. Neither of these chains actually thermalizes, in fact looking at the test MSE time series we see that both chains get stuck on the same plateau around $\text{MSE} = 10^{-3}$ and are unable to reach the MSE of the informed initialization. However, as soon as both chains reach the plateau, \hat{R} quickly drops to a value close to the order of 1 and thereafter becomes stationary, mistakenly signalling thermalization. This example exposes the problem at the heart of the multiple-chain method: the method can be fooled if the chains find themselves close to each other but far from equilibrium. Similarly, since the chains become stationary after they hit the plateau, the stationarity criterion would incorrectly predict that they have thermalized. To conclude, we have shown an example where common thermalization heuristics fail to recognize that the MCMC has not thermalized; instead, the teacher-student method detects the lack of thermalization.

B. Gibbs sampler

In this section, we show that the combination of intermediate noise posterior and Gibbs sampler is effective in sampling from the posterior by comparing it to HMC, run both on the classical and intermediate noise posteriors, and to MALA, run on the classical posterior. We provide the pseudocode for these algorithms in Appendix H. For the first set of experiments, we use the same network architecture as in the previous section. The teacher weights W_* , as well as X, X_{test} are also sampled in the same way. The intermediate noise and the classical generative process prescribe different ways of generating the labels. However, to perform a fair comparison, we use the same dataset for all MCMCs and posteriors; thus we generate the training set in a noiseless way, i.e., setting $y^\mu = f(X^\mu, W_*)$. We generate 72 datasets according to this procedure, each time using independently sampled inputs and teacher’s weights. The consequence of generating datasets in a noiseless way is that the noise level used to generate the data is different from the one in the MCMC, implying that the informed initialization will not exactly be a sample from the posterior. However, the noise is small enough that we did not observe any noticeable difference in the functioning of the teacher-student criterion.

First, we aim to characterize how often each algorithm thermalizes, when started from an uninformed initialization. Uninformed means that the network’s initialization is agnostic to the teacher’s weights. For several values of Δ , and for all the 72 datasets, we run the four algorithms (Gibbs, classical HMC, intermediate HMC, classical MALA) starting from informed and uninformed initializations. More information about the initializations and hyperparameters of these experiments is contained in Appendix I.

The left panel of figure 2 depicts the proportion of the 72 datasets in which the uninformed initialization thermalizes within 5:30h of simulation. The x -axis is the equilibrium test MSE, i.e., the average test MSE reached by the informed initialization once it becomes stationary. When Δ , and thus the test MSE, decreases, the proportion of thermalized runs drops for all algorithms, with the Gibbs sampler attaining the highest proportion, in most of the range. In the right panel, we plot the dynamics of the test error under each algorithm for a run where they all thermalize. For the same Δ s of this plot (respectively $\Delta = 10^{-3}, 4.64 \times 10^{-4}$ for the classical and intermediate noise posterior), we compute the average thermalization time among the runs that thermalize. Classical HMC, MALA, Gibbs, and intermediate HMC take, respectively on average around 130, 2700, 3200, 12500 seconds to thermalize. This shows that the classical HMC, when it thermalizes, is the fastest method, while MALA and Gibbs occupy the second and third position, with similar times. However classical HMC thermalizes about 20% less often than the Gibbs sampler. Therefore in cases where it is essential to reach equilibrium, the Gibbs sampler represents the best choice.

We now move from the abstract setting of Gaussian data to more realistic inputs and architectures. As an architecture we use a one-hidden layer MLP with 12 hidden units and ReLU activations, and a simple convolutional network (CNN) with a convolutional layer, followed by average pooling, ReLU activations, and a fully connected layer. See Appendix J for a description of both models and of the experimental details. In this setting, we resort to the stationarity criterion to check for thermalization, since the teacher-student method is inapplicable. We compare the Gibbs sampler with HMC and MALA both run on the classical posterior, picking MNIST as dataset. Figure 3 shows the test error as a

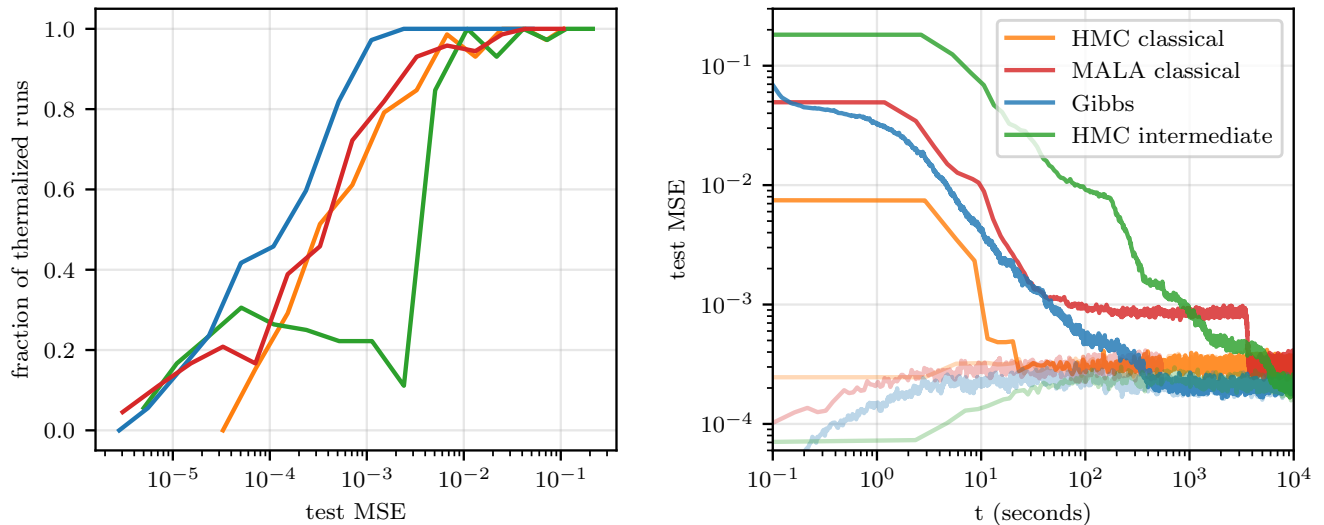


FIG. 2. Thermalization experiments on synthetic data. **Left:** Proportion of the 72 runs that thermalize plotted against the equilibrium test MSE. **Right:** Example of the dynamics of the test MSE in a particular run where all four algorithms thermalize. In order to get a similar equilibrium test MSE in the classical and intermediate noise posteriors, we pick respectively $\Delta = 10^{-3}$ and $\Delta = 4.64 \times 10^{-4}$. The transparent lines represent the informed initializations.

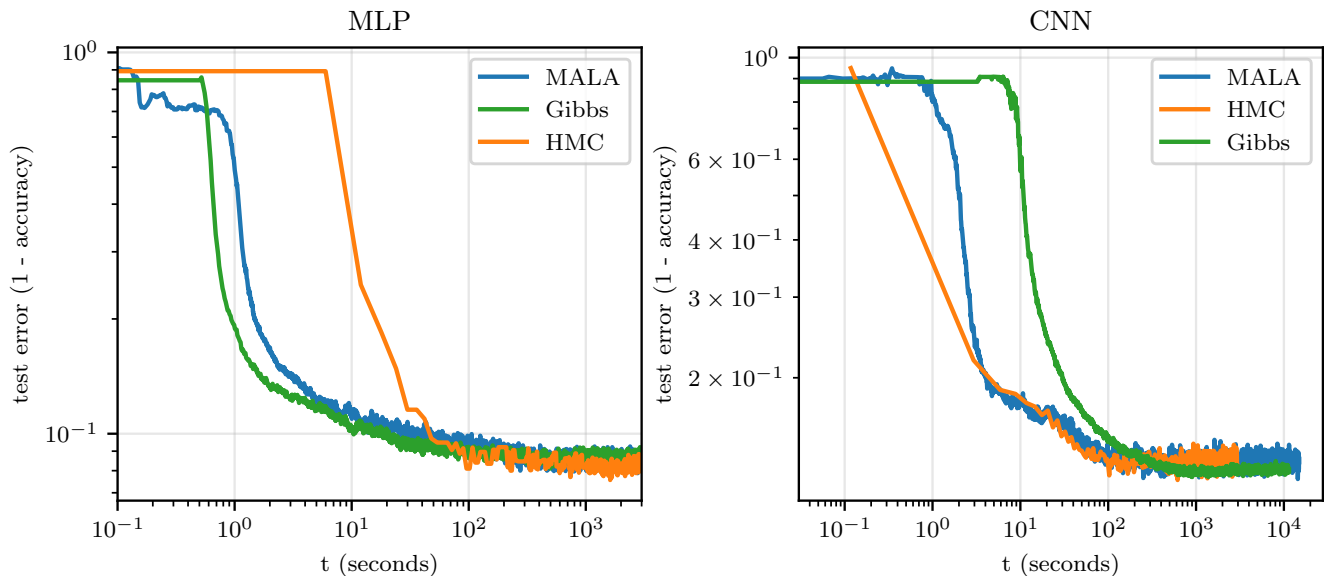


FIG. 3. Gibbs on the intermediate noise posterior and HMC, MALA both on the classical posterior, compared on MNIST. **Left:** MLP with one hidden layer with 12 hidden units. **Right:** CNN network.

function of time for the two architectures. We choose the algorithms Δ s such that they all reach a comparable test error at stationarity. We then compare the time it takes each algorithm to reach this error. The results of the experiments are depicted in figure 3. For the MLP all algorithms take approximately the same time to become stationary, around 500s. In the CNN case, after HMC and MALA reach stationarity in 100s, compared to 800s for Gibbs. We however note that for HMC and MALA to achieve these performances we had to carry out an extensive optimization over hyperparameters, thus the speed is overall comparable.

VI. CONCLUSION

In this work, we introduced the intermediate noise posterior, a probabilistic model for Bayesian learning of neural networks, along with a novel Gibbs sampler to sample from this posterior. We compared the Gibbs sampler to MALA and HMC, varying also the form of the posterior. We found that HMC and MALA both on the classical posterior and Gibbs, on the intermediate noise posterior, each have their own merits and can be considered effective in sampling the high dimensional posteriors arising from Bayesian learning of neural networks. Gibbs compares favourably to the other algorithms in terms of the ability to thermalize, moreover, no hyperparameter tuning is required, it can be applied to non-differentiable posteriors, and can be parallelized across layers.

We further proposed the teacher-student thermalization criterion: a method to obtain stringent lower bounds on the thermalization time of an MCMC, within a synthetic data setting. We first provided a simple theoretical argument to justify the method and subsequently compared it to other thermalization heuristics, finding that the teacher-student criterion consistently gives the highest lower bound to T_{therm} .

VII. ACKNOWLEDGMENT

We thank Lucas Clarté for introducing us to the blocked Gibbs sampler, and Christian Keup for the useful discussions on predictive coding and stochastic neural networks.

-
- [1] James H Albert and Siddhartha Chib. Bayesian analysis of binary and polychotomous response data. *Journal of the American statistical Association*, 88(422):669–679, 1993.
- [2] Nick Alonso, Beren Millidge, Jeff Krichmar, and Emre Neftci. A theoretical framework for inference learning. *arXiv preprint arXiv:2206.00164*, 2022.
- [3] Jean Barbier, Florent Krzakala, Nicolas Macris, Léo Miolane, and Lenka Zdeborová. Optimal errors and phase transitions in high-dimensional generalized linear models. *Proceedings of the National Academy of Sciences*, 116(12):5451–5460, 2019.
- [4] Julian Besag. Comments on “representations of knowledge in complex systems” by u. grenander and mi miller. *J. Roy. Statist. Soc. Ser. B*, 56(591-592):4, 1994.
- [5] Stephen P Brooks and Andrew Gelman. General methods for monitoring convergence of iterative simulations. *Journal of computational and graphical statistics*, 7(4):434–455, 1998.
- [6] George Casella and Edward I George. Explaining the gibbs sampler. *The American Statistician*, 46(3):167–174, 1992.
- [7] Tianqi Chen, Emily Fox, and Carlos Guestrin. Stochastic gradient hamiltonian monte carlo. In *International conference on machine learning*, pages 1683–1691. PMLR, 2014.
- [8] Adam D Cobb and Brian Jalaian. Scaling hamiltonian monte carlo inference for bayesian neural networks with symmetric splitting. *Uncertainty in Artificial Intelligence*, 2021.
- [9] Mary Kathryn Cowles and Bradley P Carlin. Markov chain monte carlo convergence diagnostics: a comparative review. *Journal of the American Statistical Association*, 91(434):883–904, 1996.
- [10] Paul Dagum and Michael Luby. Approximating probabilistic inference in bayesian belief networks is np-hard. *Artificial intelligence*, 60(1):141–153, 1993.
- [11] Joshua V. Dillon, Ian Langmore, Dustin Tran, Eugene Brevdo, Srinivas Vasudevan, Dave Moore, Brian Patton, Alex Alemi, Matt Hoffman, and Rif A. Saurous. Tensorflow distributions, 2017.
- [12] Simon Duane, Anthony D Kennedy, Brian J Pendleton, and Duncan Roweth. Hybrid monte carlo. *Physics letters B*, 195(2):216–222, 1987.
- [13] Y Fan, Stephen P Brooks, and Andrew Gelman. Output assessment for monte carlo simulations via the score statistic. *Journal of Computational and Graphical Statistics*, 15(1):178–206, 2006.
- [14] Sylvia Frühwirth-Schnatter and Rudolf Frühwirth. Data augmentation and mcmc for binary and multinomial logit models. In *Statistical modelling and regression structures*, pages 111–132. Springer, 2010.
- [15] Crispin W Gardiner et al. *Handbook of stochastic methods*, volume 3. springer Berlin, 1985.
- [16] Andrew Gelman and Donald B Rubin. Inference from iterative simulation using multiple sequences. *Statistical science*, pages 457–472, 1992.
- [17] Stuart Geman and Donald Geman. Stochastic relaxation, gibbs distributions, and the bayesian restoration of images. *IEEE Transactions on pattern analysis and machine intelligence*, PAMI-6(6):721–741, 1984.
- [18] Ethan Goan and Clinton Fookes. Bayesian neural networks: An introduction and survey. In *Case Studies in Applied Bayesian Data Science*, pages 45–87. Springer, 2020.
- [19] Jackson Gorham and Lester Mackey. Measuring sample quality with stein’s method. *Advances in Neural Information Processing Systems*, 28, 2015.
- [20] Jackson Gorham and Lester Mackey. Measuring sample quality with kernels. In *International Conference on Machine Learning*, pages 1292–1301. PMLR, 2017.
- [21] Leonhard Held and Chris C Holmes. Bayesian auxiliary variable models for binary and multinomial regression. *Bayesian analysis*, 1(1):145–168, 2006.
- [22] Matthew D Hoffman, Andrew Gelman, et al. The no-u-turn sampler: adaptively setting path lengths in hamiltonian monte carlo. *J. Mach. Learn. Res.*, 15(1):1593–1623, 2014.
- [23] Pavel Izmailov, Sharad Vikram, Matthew D Hoffman, and Andrew Gordon Gordon Wilson. What are bayesian neural network posteriors really like? In *International conference on machine learning*, pages 4629–4640. PMLR, 2021.
- [24] Laurent Valentin Jospin, Hamid Laga, Farid Boussaid, Wray Buntine, and Mohammed Bennamoun. Hands-on bayesian neural networks—a tutorial for deep learning users. *IEEE Computational Intelligence Magazine*, 17(2):29–48, 2022.
- [25] Alex Kendall and Yarin Gal. What uncertainties do we need in bayesian deep learning for computer vision? *Advances in neural information processing systems*, 30, 2017.
- [26] Mohammad Khan, Didrik Nielsen, Voot Tangkaratt, Wu Lin, Yarin Gal, and Akash Srivastava. Fast and scalable bayesian deep learning by weight-perturbation in adam. In *International Conference on Machine Learning*, pages 2611–2620. PMLR, 2018.
- [27] David A Levin and Yuval Peres. *Markov chains and mixing times*, volume 107. American Mathematical Soc., 2017.
- [28] Chunyuan Li, Changyou Chen, David Carlson, and Lawrence Carin. Preconditioned stochastic gradient langevin dynamics for deep neural networks. In *Thirtieth AAAI Conference on Artificial Intelligence*, 2016.
- [29] Yi-An Ma, Tianqi Chen, and Emily Fox. A complete recipe for stochastic gradient mcmc. *Advances in neural information processing systems*, 28, 2015.
- [30] David JC MacKay. A practical bayesian framework for backpropagation networks. *Neural computation*, 4(3):448–472, 1992.
- [31] Wesley J Maddox, Pavel Izmailov, Timur Garipov, Dmitry P Vetrov, and Andrew Gordon Wilson. A simple baseline for bayesian uncertainty in deep learning. *Advances in Neural Information Processing Systems*, 32, 2019.
- [32] Martin Magris and Alexandros Iosifidis. Bayesian learning for neural networks: an algorithmic survey. *arXiv preprint arXiv:2211.11865*, 2022.

- [33] Nicholas Metropolis, Arianna W Rosenbluth, Marshall N Rosenbluth, Augusta H Teller, and Edward Teller. Equation of state calculations by fast computing machines. *The journal of chemical physics*, 21(6):1087–1092, 1953.
- [34] Marc Mezard and Andrea Montanari. *Information, physics, and computation*. Oxford University Press, 2009.
- [35] Beren Millidge, Tommaso Salvatori, Yuhang Song, Rafal Bogacz, and Thomas Lukasiewicz. Predictive coding: Towards a future of deep learning beyond backpropagation? *arXiv preprint arXiv:2202.09467*, 2022.
- [36] Beren Millidge, Anil Seth, and Christopher L Buckley. Predictive coding: a theoretical and experimental review. *arXiv preprint arXiv:2107.12979*, 2021.
- [37] Radford M Neal. Learning stochastic feedforward networks. *Department of Computer Science, University of Toronto*, 64(1283):1577, 1990.
- [38] Radford M Neal. Connectionist learning of belief networks. *Artificial intelligence*, 56(1):71–113, 1992.
- [39] Radford M Neal. *Bayesian learning for neural networks*, volume 118. Springer Science & Business Media, 2012.
- [40] Christopher Nemeth and Paul Fearnhead. Stochastic gradient markov chain monte carlo. *Journal of the American Statistical Association*, 116(533):433–450, 2021.
- [41] Mark EJ Newman and Gerard T Barkema. *Monte Carlo methods in statistical physics*. Clarendon Press, 1999.
- [42] Tapani Raiko, Mathias Berglund, Guillaume Alain, and Laurent Dinh. Techniques for learning binary stochastic feedforward neural networks. *arXiv preprint arXiv:1406.2989*, 2014.
- [43] Gareth O Roberts and Richard L Tweedie. Exponential convergence of langevin distributions and their discrete approximations. *Bernoulli*, pages 341–363, 1996.
- [44] Mrinank Sharma, Sebastian Farquhar, Eric Nalisnick, and Tom Rainforth. Do bayesian neural networks need to be fully stochastic? *arXiv preprint arXiv:2211.06291*, 2022.
- [45] Charlie Tang and Russ R Salakhutdinov. Learning stochastic feedforward neural networks. *Advances in Neural Information Processing Systems*, 26, 2013.
- [46] Mattias Teye, Hossein Azizpour, and Kevin Smith. Bayesian uncertainty estimation for batch normalized deep networks. In *International Conference on Machine Learning*, pages 4907–4916. PMLR, 2018.
- [47] Naftali Tishby, Esther Levin, and Sara A Solla. Consistent inference of probabilities in layered networks: Predictions and generalization. In *International Joint Conference on Neural Networks*, volume 2, pages 403–409. IEEE New York, 1989.
- [48] Cédric Villani et al. *Optimal transport: old and new*, volume 338. Springer, 2009.
- [49] Hao Wang, Xingjian Shi, and Dit-Yan Yeung. Natural-parameter networks: A class of probabilistic neural networks. *Advances in neural information processing systems*, 29, 2016.
- [50] Hao Wang and Dit-Yan Yeung. A survey on bayesian deep learning. *ACM Computing Surveys (CSUR)*, 53(5):1–37, 2020.
- [51] Max Welling and Yee W Teh. Bayesian learning via stochastic gradient langevin dynamics. In *Proceedings of the 28th international conference on machine learning (ICML-11)*, pages 681–688, 2011.
- [52] Florian Wenzel, Kevin Roth, Bastiaan S Veeling, Jakub Światkowski, Linh Tran, Stephan Mandt, Jasper Snoek, Tim Salimans, Rodolphe Jenatton, and Sebastian Nowozin. How good is the bayes posterior in deep neural networks really? *arXiv preprint arXiv:2002.02405*, 2020.
- [53] James CR Whittington and Rafal Bogacz. An approximation of the error backpropagation algorithm in a predictive coding network with local hebbian synaptic plasticity. *Neural computation*, 29(5):1229–1262, 2017.
- [54] Andrew G Wilson and Pavel Izmailov. Bayesian deep learning and a probabilistic perspective of generalization. *Advances in neural information processing systems*, 33:4697–4708, 2020.
- [55] Anqi Wu, Sebastian Nowozin, Edward Meeds, Richard E Turner, Jose Miguel Hernandez-Lobato, and Alexander L Gaunt. Deterministic variational inference for robust bayesian neural networks. *arXiv preprint arXiv:1810.03958*, 2018.
- [56] Tianyuan Yu, Yongxin Yang, Da Li, Timothy Hospedales, and Tao Xiang. Simple and effective stochastic neural networks. In *Proceedings of the AAAI Conference on Artificial Intelligence*, volume 35, pages 3252–3260, 2021.
- [57] Lenka Zdeborová and Florent Krzakala. Statistical physics of inference: Thresholds and algorithms. *Advances in Physics*, 65(5):453–552, 2016.
- [58] Arnold Zellner and Chung-Ki Min. Gibbs sampler convergence criteria. *Journal of the American Statistical Association*, 90(431):921–927, 1995.
- [59] Ruqi Zhang, Chunyuan Li, Jianyi Zhang, Changyou Chen, and Andrew Gordon Wilson. Cyclical stochastic gradient mcmc for bayesian deep learning. *arXiv preprint arXiv:1902.03932*, 2019.

Appendix A: Multiple chain convergence method (or \hat{R} statistic)

In this appendix, we recall the details of the \hat{R} statistic, first introduced in [16] and [5]. The method is based on running M parallel MCMCs. Let $\{\theta_{mn} : m \in [M], n \in [N]\}$ be the Markov chains states. θ_{mn} here indicates the state of the m -th chain after n steps. The \hat{R} statistics is formulated in terms of an arbitrary function $\psi(\theta)$. We define \hat{R} in the following way

$$\bar{\psi}_{m\cdot} := \frac{1}{N} \sum_n \psi(\theta_{mn}); \quad \bar{\psi}_{\cdot\cdot} := \frac{1}{MN} \sum_{m,n} \psi(\theta_{mn}); \quad (\text{A1})$$

$$\frac{B}{N} := \frac{1}{M-1} \sum_m (\bar{\psi}_{m\cdot} - \bar{\psi}_{\cdot\cdot})^2; \quad (\text{A2})$$

$$W := \frac{1}{M(N-1)} \sum_{m,n} (\psi(\theta_{mn}) - \bar{\psi}_{m\cdot})^2; \quad (\text{A3})$$

$$\hat{\sigma}_+^2 := \frac{N-1}{N} W + \frac{B}{N}; \quad (\text{A4})$$

$$\hat{R} := \frac{M+1}{M} \frac{\hat{\sigma}_+^2}{W} - \frac{N-1}{MN}. \quad (\text{A5})$$

W estimates the within-chain variance (averaged over all chains). $\hat{\sigma}_+^2$ instead is the unbiased estimator for the variance, obtained by pooling all samples from different chains. \hat{R} is essentially $\frac{\hat{\sigma}_+^2}{W}$, apart from factors that vanish when $N, M \rightarrow \infty$. If the chains are far apart from each other then $\hat{\sigma}_+^2 \gg W$, and hence $\hat{R} \gg 1$. Instead, if all chains are close to each other then \hat{R} will be close to 1. \hat{R} can be used to derive a lower bound to the thermalization time: when all M chains have thermalized \hat{R} should be close to 1, as samples from different chains should be indistinguishable, and thus have the same variance as samples from a single chain.

Appendix B: Teacher student criterion numerical experiments

In this appendix, we report the details of the experiments presented in V A. Recall that a synthetic dataset was generated using a teacher network with Gaussian weights, and according to the intermediate noise generative process (7). Then the Gibbs sampler was used to sample from the resulting posterior. We precise that all parameters of the Gibbs sampler (i.e. all the Δ s and λ s) match those of the generative process. The Gibbs sampler was run on four chains: one with informed initialization, one initialized at zero, and two chains with independent random initializations. For the random initializations the weights of the student are sampled from the prior (with the same λ s as the teacher), then the pre- and post-activations are computed using the intermediate noise generative process (7), with noises ϵ , independent from those of the teacher. The zero-initialized chain plausibly thermalizes, while the randomly initialized ones do not. We briefly comment on how the \hat{R} statistic and the score statistics were computed.

1. \hat{R} statistic

In the notation of A, θ is given by $\{W^{(1)}, b^{(1)}, Z^{(2)}, X^{(2)}, W^{(2)}, b^{(2)}\}$. Next we have to pick the (possibly vector-valued) function $\psi(\theta)$. One possible choice is to use the weights, e.g., $\psi(\theta) = W^{(1)}$. However, due to the permutational symmetry between the neurons in the hidden layer, this gives $\hat{R} \gg 1$ even when the MCMC has thermalized. Hence one must focus on quantities that are invariant to this symmetry. A natural choice is the student output on the test set. We pick $\psi(\theta) \in \mathbb{R}^{n_{\text{test}}}$, with $\psi(\theta) = f(X_{\text{test}}, W)$ and f as in (11). We record these vectors along the simulation at times evenly spaced by 100 MCMC steps. We split the samples into blocks of 50 consecutive measurements. We then compute the \hat{R} statistic on each block (hence $N = 50$). Since the function ψ we are using returns an n_{test} dimensional output, \hat{R} will also be n_{test} dimensional. In figure 1 we then decided to plot the average (over the test set) value of \hat{R} . In other words, calling \hat{R}_τ^ν the value of \hat{R} computed on the τ -th block and the ν -th test sample, what we plot are the pairs $\left(t_\tau, \frac{1}{n_{\text{test}}} \sum_{\nu=1}^{n_{\text{test}}} \hat{R}_\tau^\nu\right)$, with t_τ being the average time within block τ . In principle the whole distribution of \hat{R} is interesting. Figure 4 shows the evolution of the 25th, 50th, 75th and 95th percentiles of \hat{R} . Recall that the two chains in the left panel thermalize, while those in the right panel are actually very far from equilibrium. Even if the distribution in the right panel is more shifted away from one than the distribution in the left panel, we still think

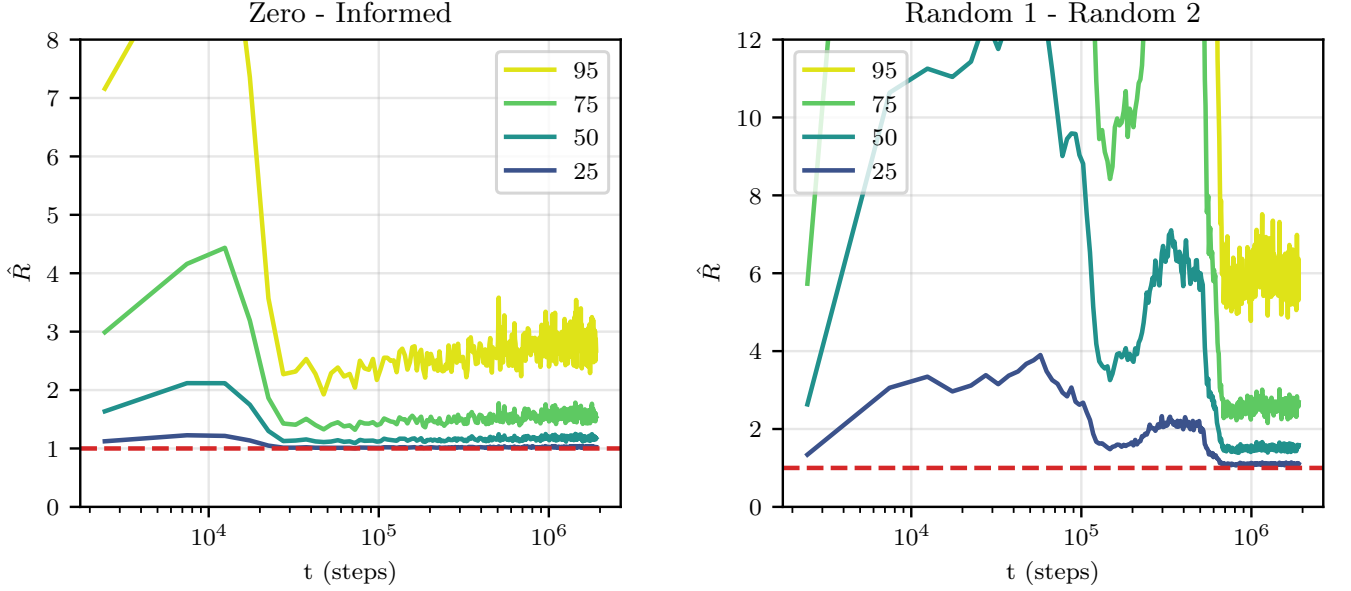


FIG. 4. Percentiles of \hat{R} as a function of time. A line marked with the number k in the legend represents how the k -th percentile of \hat{R} changes throughout the simulation. The data comes from the same simulation that was used for computing the average \hat{R} in figure 1. The red dashed horizontal line is placed at a height of 1, the value that \hat{R} should approach when the chains are close to each other. **Left:** percentiles of \hat{R} , computed on two chains with respectively zero and informed initialization. **Right:** percentiles when computing \hat{R} from two chains independently initialized at random.

that the sudden drop from a higher value and the subsequent stationarity could be interpreted as the chains having thermalized.

2. Score method

If a MCMC has thermalized then the gradient of the log posterior must have mean zero, hence the time series of each of its coordinates will have to oscillate around zero. In figure 1 we plot $U = \Delta \frac{1}{d_1 d_2} \sum_{i=1}^{d_1} \sum_{\alpha=1}^{d_2} \frac{\partial \log P}{\partial W_{\alpha i}^{(1)}}$, where P indicates the posterior distribution; this is the score rescaled by Δ and averaged over the first layer weights. We also tried taking the gradient with respect to the second layer weights $W^{(2)}$, or with respect to $Z^{(2)}$. The results do not change significantly and the score methods keep severely underestimating the thermalization time.

Appendix C: Gibbs sampler derivation

In this appendix, we provide the details of the derivation of the Gibbs sampler algorithm in the case of an MLP without biases. In order, we will derive equations (8), (9) and (10).

For $X^{(\ell)}$ we see that the conditional distribution factorizes over samples $\mu \in [n]$.

$$\begin{aligned}
 P(X^{(\ell)\mu} | \text{All}) &= P(X^{(\ell)\mu} | Z^{(\ell)\mu}, W^{(\ell)}, Z^{(\ell+1)\mu}) = \frac{P(X^{(\ell)\mu}, Z^{(\ell+1)\mu} | W^{(\ell)}, Z^{(\ell)\mu})}{P(Z^{(\ell)\mu} | W^{(\ell)}, Z^{(\ell-1)\mu})} = \\
 &= \frac{P(Z^{(\ell+1)\mu} | W^{(\ell)}, X^{(\ell)\mu}) P(X^{(\ell)\mu} | W^{(\ell)}, Z^{(\ell)\mu})}{P(Z^{(\ell)\mu} | W^{(\ell)}, Z^{(\ell-1)\mu})} \propto P(Z^{(\ell+1)\mu} | W^{(\ell)}, X^{(\ell)\mu}) P(X^{(\ell)\mu} | Z^{(\ell)\mu}) \\
 &= \mathcal{N}(Z^{(\ell+1)\mu} | W^{(\ell)}, X^{(\ell)\mu}, \Delta_Z^{(\ell+1)} \mathbb{1}_{d_{\ell+1}}) \mathcal{N}(X^{(\ell)\mu} | \sigma(Z^{(\ell)\mu}), \Delta_X^{(\ell)} \mathbb{1}_{d_\ell}) = \mathcal{N}(X^{(\ell)\mu} | m_X^{(\ell)\mu}, \Sigma_X^{(\ell)}), \quad (\text{C1})
 \end{aligned}$$

with $\Sigma^{(X_\ell)} = \left(\frac{1}{\Delta_Z^{(\ell+1)}} W^{(\ell)T} W^{(\ell)} + \frac{1}{\Delta_X^{(\ell)}} \mathbb{1}_{d_\ell} \right)^{-1}$, and $(m^{(X_\ell)})^\mu = \Sigma^{(X_\ell)} \left(\frac{1}{\Delta_X^{(\ell)}} \sigma(Z^{(\ell)\mu}) + \frac{1}{\Delta_Z^{(\ell+1)}} W^{(\ell)T} Z^{(\ell+1)\mu} \right)$. In the derivation we used that $P(X^{(\ell)} | W^{(\ell)}, Z^{(\ell)}) = P(X^{(\ell)} | Z^{(\ell)})$. We see that the conditional distribution of $X^{(\ell)}$ is a multivariate Gaussian, hence it is possible to sample from it efficiently on a computer.

Algorithm 2 Parallel Gibbs sampler for MLP. The expression **for parallel** indicates that all iterations of the loop can be executed in parallel.

Input: training inputs X , training labels y , noise variances $\{\Delta_Z^{(\ell)}\}_{\ell=2}^{L+1}$, $\{\Delta_X^{(\ell)}\}_{\ell=2}^L$, prior inverse variances $\{\lambda_W^{(\ell)}\}_{\ell=1}^L$, initial condition $\{X^{(\ell)}\}_{\ell=2}^L, \{W^{(\ell)}\}_{\ell=1}^L, \{Z^{(\ell)}\}_{\ell=2}^L$, length of the simulation t_{\max}

Output: a sequence S of samples

$X^{(1)} \leftarrow X$

$Z^{(L+1)} \leftarrow y$

$S \leftarrow \{\{W^{(\ell)}\}_{\ell=1}^L, \{X^{(\ell)}\}_{\ell=2}^L, \{Z^{(\ell)}\}_{\ell=2}^L\}$

for $t = 1, \dots, t_{\max}$ **do**

for parallel $\ell = 2, \dots, L$ **do**

$X^{(\ell)} \sim P(X^{(\ell)} | Z^{(\ell)}, W^{(\ell)}, Z^{(\ell+1)})$ ▷ (8)

end for

for parallel $\ell = 1, \dots, L$ **do**

$W^{(\ell)} \sim P(W^{(\ell)} | X^{(\ell)}, Z^{(\ell+1)})$ ▷ (9)

end for

for parallel $\ell = 2, \dots, L$ **do**

$Z^{(\ell)} \sim P(Z^{(\ell)} | X^{(\ell-1)}, W^{(\ell-1)}, X^{(\ell)})$ ▷ (10)

end for

$S.append(\{W^{(\ell)}\}_{\ell=1}^L, \{X^{(\ell)}\}_{\ell=2}^L, \{Z^{(\ell)}\}_{\ell=2}^L)$

end for

For $W^{(\ell)}$ we exploit that the conditional factorizes over the rows $\alpha \in [d_{\ell+1}]$.

$$P(W_\alpha^{(\ell)} | \text{All}) = P(W_\alpha^{(\ell)} | X^{(\ell)}, Z_\alpha^{(\ell+1)}) = \frac{P(Z_\alpha^{(\ell+1)} | W_\alpha^{(\ell)}, X^{(\ell)}) P(W_\alpha^{(\ell)} | X^{(\ell)})}{P(Z_\alpha^{(\ell+1)} | X^{(\ell)})} \quad (\text{C2})$$

$$\propto P(Z_\alpha^{(\ell+1)} | W_\alpha^{(\ell)}, X^{(\ell)}) P(W_\alpha^{(\ell)}) = \mathcal{N}(Z_\alpha^{(\ell+1)} | X^{(\ell)} W_\alpha^{(\ell)}, \Delta_Z^{(\ell+1)}) \mathcal{N}(W_\alpha^{(\ell)} | 0, \mathbb{I}_{d_\ell} / \lambda_W^{(\ell)}) \quad (\text{C3})$$

$$= \mathcal{N}(W_\alpha^{(\ell)} | m_W^{(\ell)}, \Sigma_W^{(\ell)}), \quad (\text{C4})$$

with $\Sigma_W^{(\ell)} = \left(\frac{1}{\Delta_Z^{(\ell+1)}} X^{(\ell)T} X^{(\ell)} + \lambda_W^{(\ell)} \mathbb{I}_d \right)^{-1}$, and $(m_W^{(\ell)})_\alpha = \frac{1}{\Delta_Z^{(\ell+1)}} \Sigma_W^{(\ell)} X^{(\ell)T} Z_\alpha^{(\ell+1)}$. Once again the conditional distribution of $W^{(\ell)}$ is a multivariate Gaussian.

In the case of $Z^{(\ell+1)}$ the conditional factorizes both over samples and over coordinates. We have

$$P(Z_\alpha^{(\ell+1)\mu} | \text{All}) = P(Z_\alpha^{(\ell+1)\mu} | X_\alpha^{(\ell+1)\mu}, W_\alpha^{(\ell)}, X^{(\ell)\mu}) = \frac{P(Z_\alpha^{(\ell+1)\mu}, X_\alpha^{(\ell+1)\mu} | W_\alpha^{(\ell)}, X^{(\ell)\mu})}{P(X_\alpha^{(\ell+1)\mu} | W_\alpha^{(\ell)}, X^{(\ell)\mu})} \quad (\text{C5})$$

$$= \frac{P(Z_\alpha^{(\ell+1)\mu} | X_\alpha^{(\ell)\mu}, W_\alpha^{(\ell)}) P(X_\alpha^{(\ell+1)\mu} | Z_\alpha^{(\ell+1)\mu})}{P(X_\alpha^{(\ell+1)\mu} | W_\alpha^{(\ell)}, X^{(\ell)\mu})} \quad (\text{C6})$$

$$\propto P(Z_\alpha^{(\ell+1)\mu} | X_\alpha^{(\ell)\mu}, W_\alpha^{(\ell)}) P(X_\alpha^{(\ell+1)\mu} | Z_\alpha^{(\ell+1)\mu}) \quad (\text{C7})$$

$$= \mathcal{N}(Z_\alpha^{(\ell+1)\mu} | W_\alpha^{(\ell)T} X^{(\ell)\mu}, \Delta_Z^{(\ell+1)}) \mathcal{N}(X_\alpha^{(\ell+1)\mu} | \sigma(Z_\alpha^{(\ell+1)\mu}), \Delta_X^{(\ell+1)}) \propto \quad (\text{C8})$$

$$\propto \exp \left[-\frac{1}{2\Delta_Z^{(\ell+1)}} \left(Z_\alpha^{(\ell+1)\mu} - W_\alpha^{(\ell)T} X^{(\ell)\mu} \right)^2 - \frac{1}{2\Delta_X^{(\ell+1)}} \left(\sigma(Z_\alpha^{(\ell+1)\mu}) - X_\alpha^{(\ell+1)\mu} \right)^2 \right]. \quad (\text{C9})$$

Appendix D: Parallelizability of the Gibbs sampler

In this appendix, we present a version of the Gibbs sampler that is parallelized across layers. Its pseudocode is reported in algorithm 2.

Notice that operations within each of the inner loops over ℓ can be executed in parallel, as there are no cross dependencies between different ℓ s: for example, one can sample $X^{(2)}, X^{(3)}$ and $X^{(4)}$ in parallel. This implies that, provided that we have enough computing power, the running time of the algorithm can be made independent of the depth of the network. Also updating a variable in layer ℓ only requires knowing the state of variables in adjacent layers (i.e. $\ell - 1, \ell + 1$), thus from a memory point of view the variables can be stored in different nodes in a cluster, with minimal communication between nodes necessary. Suppose for example that the depth of the network, L , is even and that we store the variables from X to $Z^{(L/2)}$ in the first node, and the variables from $X^{(L/2)}$ to y in the second. Then, when running the Gibbs sampler, it is only necessary to synchronize $Z^{(L/2)}$ and $X^{(L/2)}$ between the nodes.

Appendix E: Sampling from $P(Z_\alpha^{(\ell+1)\mu} | X_\alpha^{(\ell+1)\mu}, W_\alpha^{(\ell)}, X^{(\ell)\mu})$

In this section, we specify how to sample the pre-activations $Z^{(\ell)}$ in the Gibbs sampler. Given an activation function $\sigma(\cdot)$, our goal is to sample the one dimensional random variable $Z_\alpha^{(\ell+1)\mu}$ with distribution

$$P(Z_\alpha^{(\ell+1)\mu} | X_\alpha^{(\ell+1)\mu}, W_\alpha^{(\ell)}, X^{(\ell)\mu}) = \frac{1}{\mathcal{Z}} \exp \left[-\frac{1}{2\Delta_Z^{(\ell+1)}} \left(Z_\alpha^{(\ell+1)\mu} - W_\alpha^{(\ell)T} X^{(\ell)\mu} \right)^2 \right] \quad (\text{E1})$$

$$\left[-\frac{1}{2\Delta_X^{(\ell+1)}} \left(\sigma(Z_\alpha^{(\ell+1)\mu}) - X_\alpha^{(\ell+1)\mu} \right)^2 \right] \quad (\text{E2})$$

We shall now provide sampling algorithm for various activation functions.

$$1. \quad \sigma(z) = \max(0, z)$$

We have two cases depending on whether $Z_\alpha^{(\ell+1)\mu}$ is positive or negative.

Consider first the case $Z_\alpha^{(\ell+1)\mu} \leq 0$.

In this case $P(Z_\alpha^{(\ell+1)\mu} | X_\alpha^{(\ell+1)\mu}, W_\alpha^{(\ell)}, X^{(\ell)\mu}) \propto \mathcal{N}(Z_\alpha^{(\ell+1)\mu} | W_\alpha^{(\ell)T} X^{(\ell)\mu}, \Delta_Z^{(\ell+1)})$, hence the term coming from $X^{(\ell+1)}$ does not appear. The mass of this part of the distribution is

$$\mathcal{Z}_- = \int_{-\infty}^0 \exp \left[-\frac{1}{2\Delta_Z^{(\ell+1)}} z^2 + \frac{1}{\Delta_Z^{(\ell+1)}} z W_\alpha^{(\ell)T} X^{(\ell)\mu} \right] dz \quad (\text{E3})$$

$$= \sqrt{\frac{\pi \Delta_Z^{(\ell+1)}}{2}} e^{\frac{1}{2\Delta_Z^{(\ell+1)}} (W_\alpha^{(\ell)T} X^{(\ell)\mu})^2} \operatorname{erfc} \left(\frac{W_\alpha^{(\ell)T} X^{(\ell)\mu}}{\sqrt{2\Delta_Z^{(\ell+1)}}} \right) \quad (\text{E4})$$

We now look at the case $Z_\alpha^{(\ell+1)\mu} > 0$.

$$P(Z_\alpha^{(\ell+1)\mu} | X_\alpha^{(\ell+1)\mu}, W_\alpha^{(\ell)}, X^{(\ell)\mu}) \propto \mathcal{N}(Z_\alpha^{(\ell+1)\mu} | W_\alpha^{(\ell)T} X^{(\ell)\mu}, \Delta_Z^{(\ell+1)}) \times \quad (\text{E5})$$

$$\times \mathcal{N}(X_\alpha^{(\ell+1)\mu} | Z_\alpha^{(\ell+1)\mu}, \Delta_X^{(\ell+1)}) \propto \quad (\text{E6})$$

$$\propto \mathcal{N} \left(Z_\alpha^{(\ell+1)\mu} \left| \frac{\Delta_X^{(\ell+1)} W_\alpha^{(\ell)T} X^{(\ell)\mu} + \Delta_Z^{(\ell+1)} X_\alpha^{(\ell+1)\mu}}{\Delta_X^{(\ell+1)} + \Delta_Z^{(\ell+1)}}, \frac{\Delta_X^{(\ell+1)} \Delta_Z^{(\ell+1)}}{\Delta_X^{(\ell+1)} + \Delta_Z^{(\ell+1)}} \right. \right). \quad (\text{E7})$$

The mass of this part is

$$\mathcal{Z}_+ = \int_0^\infty \exp \left[-\frac{1}{2} \left(\frac{\Delta_X^{(\ell+1)} + \Delta_Z^{(\ell+1)}}{\Delta_X^{(\ell+1)} \Delta_Z^{(\ell+1)}} \right) z^2 + z \left(\frac{X_\alpha^{(\ell+1)\mu}}{\Delta_X^{(\ell+1)}} + \frac{W_\alpha^{(\ell)T} X^{(\ell)\mu}}{\Delta_Z^{(\ell+1)}} \right) \right] dz \quad (\text{E8})$$

$$= \sqrt{\frac{\pi \Delta_X^{(\ell+1)} \Delta_Z^{(\ell+1)}}{2(\Delta_X^{(\ell+1)} + \Delta_Z^{(\ell+1)})}} \exp \left[\frac{\left(\Delta_Z^{(\ell+1)} X_\alpha^{(\ell+1)\mu} + \Delta_X^{(\ell+1)} W_\alpha^{(\ell)T} X^{(\ell)\mu} \right)^2}{2(\Delta_X^{(\ell+1)} + \Delta_Z^{(\ell+1)}) \Delta_X^{(\ell+1)} \Delta_Z^{(\ell+1)}} \right] \times \quad (\text{E9})$$

$$\times \left[\operatorname{erf} \left(\frac{\Delta_Z^{(\ell+1)} X_\alpha^{(\ell+1)\mu} + \Delta_X^{(\ell+1)} W_\alpha^{(\ell)T} X^{(\ell)\mu}}{\sqrt{2(\Delta_X^{(\ell+1)} + \Delta_Z^{(\ell+1)}) \Delta_X^{(\ell+1)} \Delta_Z^{(\ell+1)}}} \right) + 1 \right] \quad (\text{E10})$$

Then one has $\mathcal{Z} = \mathcal{Z}_+ + \mathcal{Z}_-$. The probability of having $Z_\alpha^{(\ell+1)\mu} < 0$ is $p_- = \frac{\mathcal{Z}_-}{\mathcal{Z}} = \frac{1}{1 + \frac{\mathcal{Z}_+}{\mathcal{Z}_-}}$

a. Sampling

First draw a bernoulli variable $r \sim \text{Bernoulli}(p_-)$. If $r = 1$ sample a negative truncated normal from the $z < 0$ distribution. If $r = 0$ sample a positive truncated normal from the $z > 0$ distribution.

2. $\sigma(z) = \text{sign}(z)$

If $Z_\alpha^{(\ell+1)\mu} > 0$ (resp. < 0) one ends up sampling from positive (resp. negative) part of the following Gaussian

$$P(Z_\alpha^{(\ell+1)\mu} | X_\alpha^{(\ell+1)\mu}, W_\alpha^{(\ell)}, X^{(\ell)\mu}) \propto \quad (\text{E11})$$

$$\propto \frac{1}{Z} \exp \left[\frac{1}{\Delta_Z^{(\ell+1)}} Z_\alpha^{(\ell+1)\mu} W_\alpha^{(\ell)T} X^{(\ell)\mu} - \frac{1}{2\Delta_Z^{(\ell+1)}} (Z_\alpha^{(\ell+1)\mu})^2 \right] \propto \mathcal{N}(W_\alpha^{(\ell)T} X^{(\ell)\mu}, \Delta_Z^{(\ell+1)}) \quad (\text{E12})$$

We now compute the normalization associated to the positive and negative parts

Positive part

$$\mathcal{Z}_+ = \int_0^\infty \exp \left[\frac{1}{\Delta_X^{(\ell+1)}} X_\alpha^{(\ell+1)\mu} + \frac{1}{\Delta_Z^{(\ell+1)}} Z_\alpha^{(\ell+1)\mu} W_\alpha^{(\ell)T} X^{(\ell)\mu} - \frac{1}{2\Delta_Z^{(\ell+1)}} (Z_\alpha^{(\ell+1)\mu})^2 \right] = \quad (\text{E13})$$

$$= \sqrt{\frac{\pi \Delta_Z^{(\ell+1)}}{2}} \exp \left[\frac{1}{\Delta_X^{(\ell+1)}} X_\alpha^{(\ell+1)\mu} \right] \exp \left(\frac{(W_\alpha^{(\ell)T} X^{(\ell)\mu})^2}{2\Delta_Z^{(\ell+1)}} \right) \left[1 + \text{erf} \left(\frac{W_\alpha^{(\ell)T} X^{(\ell)\mu}}{\sqrt{2\Delta_Z^{(\ell+1)}}} \right) \right] \quad (\text{E14})$$

Negative part

$$\mathcal{Z}_- = \int_{-\infty}^0 \exp \left[-\frac{1}{\Delta_X^{(\ell+1)}} X_\alpha^{(\ell+1)\mu} + \frac{1}{\Delta_Z^{(\ell+1)}} Z_\alpha^{(\ell+1)\mu} W_\alpha^{(\ell)T} X^{(\ell)\mu} - \frac{1}{2\Delta_Z^{(\ell+1)}} (Z_\alpha^{(\ell+1)\mu})^2 \right] \quad (\text{E15})$$

$$= \sqrt{\frac{\pi \Delta_Z^{(\ell+1)}}{2}} \exp \left[-\frac{1}{\Delta_X^{(\ell+1)}} X_\alpha^{(\ell+1)\mu} \right] \exp \left(\frac{(W_\alpha^{(\ell)T} X^{(\ell)\mu})^2}{2\Delta_Z^{(\ell+1)}} \right) \text{erfc} \left(\frac{W_\alpha^{(\ell)T} X^{(\ell)\mu}}{\sqrt{2\Delta_Z^{(\ell+1)}}} \right) \quad (\text{E16})$$

Hence the probability of selecting the $Z < 0$ part is $p_- = 1 / \left(1 + \frac{\mathcal{Z}_+}{\mathcal{Z}_-} \right)$.

$$\frac{\mathcal{Z}_+}{\mathcal{Z}_-} = \exp \left[\frac{2}{\Delta_X^{(\ell+1)}} X_\alpha^{(\ell+1)\mu} \right] \frac{\left[1 + \text{erf} \left(\frac{W_\alpha^{(\ell)T} X^{(\ell)\mu}}{\sqrt{2\Delta_Z^{(\ell+1)}}} \right) \right]}{\text{erfc} \left(\frac{W_\alpha^{(\ell)T} X^{(\ell)\mu}}{\sqrt{2\Delta_Z^{(\ell+1)}}} \right)}$$

a. Sampling

First draw a Bernoulli variable $r \sim \text{Bernoulli}(p_-)$. If $r = 1$ sample a negative truncated normal from (E11). If $r = 0$ sample a positive truncated normal from (E11).

3. $\sigma(x) = |x|$

Both the positive and negative parts of Gaussians and we have

$$P(Z_\alpha^{(\ell+1)\mu} | X_\alpha^{(\ell+1)\mu}, W_\alpha^{(\ell)}, X^{(\ell)\mu}) \propto \begin{cases} \mathcal{N}(m_+, 1/a) & \text{if } z \geq 0 \\ \mathcal{N}(m_-, 1/a) & \text{if } z < 0 \end{cases} \quad (\text{E17})$$

with $a = \frac{\Delta_X^{(\ell+1)} + \Delta_Z^{(\ell+1)}}{\Delta_X^{(\ell+1)} \Delta_Z^{(\ell+1)}}$ and $m_\pm = \frac{\Delta_X^{(\ell+1)} W_\alpha^{(\ell)T} X^{(\ell)\mu} \pm \Delta_Z^{(\ell+1)} X_\alpha^{(\ell+1)\mu}}{\Delta_X^{(\ell+1)} + \Delta_Z^{(\ell+1)}}$. We now have to compute the masses of the positive and negative parts, we have

$$\mathcal{Z}_+ = \int_0^\infty \exp \left[\frac{1}{\Delta_X^{(\ell+1)}} X_\alpha^{(\ell+1)\mu} Z_\alpha^{(\ell+1)\mu} - \frac{1}{2\Delta_X^{(\ell+1)}} (Z_\alpha^{(\ell+1)\mu})^2 + \right] \quad (\text{E18})$$

$$+ \frac{1}{\Delta_Z^{(\ell+1)}} Z_\alpha^{(\ell+1)\mu} W_\alpha^{(\ell)T} X^{(\ell)\mu} - \frac{1}{2\Delta_Z^{(\ell+1)}} (Z_\alpha^{(\ell+1)\mu})^2 \Big] = \sqrt{\frac{\pi}{2a}} e^{q_+^2} [1 + \text{erf}(q_+)], \quad (\text{E19})$$

with a as before and $q_{\pm} = \frac{\Delta_X^{(\ell+1)} W_{\alpha}^{(\ell)T} X^{(\ell)\mu} \pm \Delta_Z^{(\ell+1)} X_{\alpha}^{(\ell+1)\mu}}{\sqrt{2(\Delta_X^{(\ell+1)} + \Delta_Z^{(\ell+1)}) \Delta_X^{(\ell+1)} \Delta_Z^{(\ell+1)}}}$. Similarly the negative part gives

$$\mathcal{Z}_- = \int_{-\infty}^0 \exp \left[-\frac{1}{\Delta_X^{(\ell+1)}} X_{\alpha}^{(\ell+1)\mu} Z_{\alpha}^{(\ell+1)\mu} - \frac{1}{2\Delta_X^{(\ell+1)}} (Z_{\alpha}^{(\ell+1)\mu})^2 + \right. \quad (\text{E20})$$

$$\left. + \frac{1}{\Delta_Z^{(\ell+1)}} Z_{\alpha}^{(\ell+1)\mu} W_{\alpha}^{(\ell)T} X^{(\ell)\mu} - \frac{1}{2\Delta_Z^{(\ell+1)}} (Z_{\alpha}^{(\ell+1)\mu})^2 \right] = \sqrt{\frac{\pi}{2a}} e^{q_-^2} \operatorname{erfc}(q_-) \quad (\text{E21})$$

We have $p_- = \frac{1}{1 + \mathcal{Z}_+ / \mathcal{Z}_-}$, with

$$\frac{\mathcal{Z}_+}{\mathcal{Z}_-} = \exp \left[\frac{2X_{\alpha}^{(\ell+1)\mu} W_{\alpha}^{(\ell)T} X^{(\ell)\mu}}{\Delta_X^{(\ell+1)} + \Delta_Z^{(\ell+1)}} \right] \frac{1 + \operatorname{erf}(q_+)}{\operatorname{erfc}(q_-)} \quad (\text{E22})$$

The sampling procedure is the same as the sign and the ReLU activation: one first draws a Bernoulli(p_-) variable and then samples either from the negative or positive truncated normal in (E17), respectively if the Bernoulli variable is one or zero.

4. Multinomial probit for multiclass classification

In the setting of multiclass classification we one hot encode the output label $y^{\mu} \in \{1, 2, \dots, C\}$, with C the number of classes. To lighten the notation, in this section we use $Z^{(L+1)} \rightarrow Z^1$, $X^{(L)} \rightarrow X$, $\Delta_Z^{(L+1)} \mapsto \Delta_Z$, $W^{(L)} \rightarrow W$. Hence we have $Z = XW^T + \epsilon_Z$, with ϵ_Z a matrix with i.i.d. elements $\mathcal{N}(0, \Delta_Z)$. We then define the output of the network to be $y^{\mu} = \arg \max_{\alpha \in [C]} Z_{\alpha}^{\mu}$. This model is also known as the multinomial probit model, and the sampling scheme we describe has been introduced in [1] and [21]. We can then do Gibbs sampling over W as usual. We are left with sampling Z . Its conditional distribution is

$$P(Z_{\mu} | y^{\mu}, W, X^{\mu}) = \frac{P(y^{\mu} | Z^{\mu}) P(Z^{\mu} | W, X)}{P(y^{\mu} | W, X)} = \quad (\text{E23})$$

$$= \frac{1}{Z} \exp \left[-\frac{1}{2\Delta(Z)} (Z_{\alpha}^{\mu} - W_{\alpha}^T X^{\mu})^2 \right] \prod_{\alpha \neq y} \Theta(Z_{y^{\mu}}^{\mu} > Z_{\alpha}^{\mu}) \quad (\text{E24})$$

Let $Z_{-\alpha}^{\mu} = (Z_1^{\mu}, \dots, Z_{\alpha-1}^{\mu}, Z_{\alpha+1}^{\mu}, \dots, Z_C^{\mu})$, i.e., the vector with coordinate α removed. We then sample Z^{μ} in coordinate wise manner. We have

$$P(Z_{y^{\mu}}^{\mu} | y^{\mu}, W, X^{\mu}, Z_{-y^{\mu}}^{\mu}) \propto \exp \left[-\frac{1}{2\Delta_Z} (Z_{y^{\mu}}^{\mu} - W_{y^{\mu}}^T X^{\mu})^2 \right] \mathbb{1} \left[Z_{y^{\mu}}^{\mu} \geq \max_{\alpha \neq y^{\mu}} Z_{\alpha}^{\mu} \right] \quad (\text{E25})$$

$$P(Z_{\alpha}^{\mu} | y^{\mu}, W, X^{\mu}, Z_{-\alpha}^{\mu}) \propto \exp \left[-\frac{1}{2\Delta_Z} (Z_{\alpha}^{\mu} - W_{\alpha}^T X^{\mu})^2 \right] \mathbb{1} [Z_{\alpha}^{\mu} \leq Z_{y^{\mu}}^{\mu}], \quad \forall \alpha \neq y^{\mu} \quad (\text{E26})$$

These distributions are truncated Gaussians so they are easy to sample. To be more precise one goes through $\alpha = 1, 2, \dots, C$ sequentially and draws Z_{α}^{μ} from (E26) or (E25).

Appendix F: Adding biases

We consider a layer of the kind $Z_{\alpha}^{(\ell+1)\mu} = W^{(\ell)T} X^{(\ell)\mu} + b_{\alpha}^{(\ell)} + \epsilon_Z^{(\ell+1)}$, with $\epsilon_Z^{(\ell+1)}$ a matrix with i.i.d. $\mathcal{N}(0, \Delta_Z^{(\ell+1)})$ elements. We suppose that the biases have a prior $b_{\alpha}^{(\ell)} \sim \mathcal{N}(0, 1/\lambda_b^{(\ell)})$. We now compute the conditional probabilities in this setting. The strategy is to use the expressions obtained before and absorb b in the previous terms. In the case of $P(W_{\alpha}^{(\ell)} | X^{(\ell)}, Z_{\alpha}^{(\ell+1)\mu})$ and $P(X^{(\ell)\mu} | Z^{(\ell)\mu} W^{(\ell)}, Z^{(\ell+1)\mu})$, one can replace $Z_{\alpha}^{(\ell+1)\mu} \rightarrow Z_{\alpha}^{(\ell+1)\mu} - b_{\alpha}^{(\ell)}$ to obtain

¹ $Z^{(L+1)}$ here are the preactivations of the last layer.

the additional conditioning on b . Moving to $P(Z_\alpha^{(\ell+1)\mu} | X_\alpha^{(\ell+1)\mu}, W_\alpha^{(\ell)}, X^{(\ell)\mu})$ one can instead do the substitution $W_\alpha^{(\ell)T} X^{(\ell)\mu} \rightarrow W_\alpha^{(\ell)T} X^{(\ell)\mu} + b_\alpha^{(\ell)}$. We are left with computing $P(b_\alpha^{(\ell)} | X^{(\ell)}, Z_\alpha^{(\ell+1)}, W_\alpha^{(\ell)})$. We have

$$P(b_\alpha^{(\ell)} | X^{(\ell)}, Z_\alpha^{(\ell+1)}, W_\alpha^{(\ell)}) \propto \quad (\text{F1})$$

$$\propto \exp \left[-\frac{1}{2\Delta_Z^{(\ell+1)}} \sum_\mu \left(Z_\alpha^{(\ell+1)\mu} - W_\alpha^{(\ell)T} X^{(\ell)\mu} - b_\alpha^{(\ell)} \right)^2 - \frac{\lambda_b^{(\ell)}}{2} (b_\alpha^{(\ell)})^2 \right] = \quad (\text{F2})$$

$$= \exp \left[-\frac{1}{2} (b_\alpha^{(\ell)})^2 \left(\lambda_b^{(\ell)} + \frac{n}{\Delta_Z^{(\ell+1)}} \right) + \frac{1}{\Delta_Z^{(\ell+1)}} b_\alpha^{(\ell)} \left(\sum_\mu Z_\alpha^{(\ell+1)\mu} - W_\alpha^{(\ell)T} X^{(\ell)\mu} \right) \right] \propto \quad (\text{F3})$$

$$\propto \mathcal{N}(b_\alpha^{(\ell)} | (m_b^{(\ell)})_\alpha, (\sigma_b^{(\ell)})^2) \quad (\text{F4})$$

with $(\sigma_b^{(\ell)})^2 = \frac{\Delta_Z^{(\ell+1)}}{n + \Delta_Z^{(\ell+1)} \lambda_b^{(\ell)}}$ and $(m_b^{(\ell)})_\alpha = \frac{1}{\Delta_Z^{(\ell+1)} \lambda_b^{(\ell)} + n} \left(\sum_\mu Z_\alpha^{(\ell+1)\mu} - W_\alpha^{(\ell)T} X^{(\ell)\mu} \right)$.

For the other variables we have

$$P(W_\alpha^{(\ell)} | X^{(\ell)}, Z_\alpha^{(\ell+1)}, b_\alpha^{(\ell)}) = \mathcal{N}(W_\alpha^{(\ell)} | m_\alpha^{(W)}, \Sigma^{(W)}), \quad (\text{F5})$$

$$P(Z_\alpha^{(\ell+1)\mu} | X_\alpha^{(\ell+1)\mu}, W_\alpha^{(\ell)}, X^{(\ell)\mu}, b_\alpha^{(\ell)}) = \exp \left[-\frac{1}{2\Delta_Z^{(\ell+1)}} \left(Z_\alpha^{(\ell+1)\mu} - W_\alpha^{(\ell)T} X^{(\ell)\mu} - b_\alpha^{(\ell)} \right)^2 \right] \quad (\text{F6})$$

$$- \frac{1}{2\Delta_X^{(\ell+1)}} \left(\sigma(Z_\alpha^{(\ell+1)\mu}) - X_\alpha^{(\ell+1)\mu} \right)^2 \Big], \quad (\text{F7})$$

$$P(X^{(\ell)\mu} | Z^{(\ell)\mu}, W^{(\ell)}, Z^{(\ell+1)\mu}, b^{(\ell)}) = \mathcal{N}(X^{(\ell)\mu} | m^{(X_\ell)\mu}, \Sigma^{(X_\ell)}) \quad (\text{F8})$$

with

$$\Sigma_W^{(\ell)} = \left(\frac{1}{\Delta_Z^{(\ell+1)}} X^{(\ell)T} X^{(\ell)} + \lambda_W^{(\ell)} \mathbb{1}_d \right)^{-1}, \quad (m_W^{(\ell)})_\alpha = \frac{1}{\Delta_Z^{(\ell+1)}} \Sigma^{(W)} X^{(\ell)T} \left(Z_\alpha^{(\ell+1)} - \mathbf{1}_n b_\alpha^{(\ell)} \right) \quad (\text{F9})$$

$$\Sigma_X^{(\ell)} = \left(\frac{1}{\Delta_Z^{(\ell+1)}} W^{(\ell)T} W^{(\ell)} + \frac{1}{\Delta_X^{(\ell)}} \mathbb{1}_{d_\ell} \right)^{-1}, \quad (\text{F10})$$

$$(m_X^{(\ell)})^\mu = \Sigma^{(X_\ell)} \left(\frac{1}{\Delta_X^{(\ell)}} \sigma(Z^{(\ell)\mu}) + \frac{1}{\Delta_Z^{(\ell+1)}} W^{(\ell)T} (Z^{(\ell+1)\mu} - b^{(\ell)}) \right). \quad (\text{F11})$$

Here $\mathbf{1}_n$ is the vector of length n whose coordinates are all ones.

There is an alternative way of sampling b . One can consider $b^{(\ell)}$ as the $d_\ell + 1$ th column of an extended weight matrix $\tilde{W}^{(\ell)} = [W^{(\ell)} | b^{(\ell)}]$. These extended weights act on $\tilde{X}^{(\ell)} = [X^{(\ell)} | \mathbf{1}_n]$, a $n \times (d_\ell + 1)$ matrix, whose last column contains all ones. The generative process, with biases included, can be written as $Z^{(\ell+1)} = \tilde{X} \tilde{W}^T + \epsilon_Z^{(\ell+1)}$, with ϵ_Z an $n \times d_{\ell+1}$ matrix with i.i.d. $\mathcal{N}(0, \Delta_Z^{(\ell+1)})$ elements. One can compute (and later sample from) $P(\tilde{W}^{(\ell)} | \tilde{X}^{(\ell)}, Z^{(\ell+1)})$, following the same procedure that we used to compute (9). The only difference is that the prior variance is not uniform over \tilde{W} : one will instead have both $\lambda_W^{(\ell)}$ and $\lambda_b^{(\ell)}$.

Appendix G: Gibbs sampling for convolutional neural networks

In order to implement the Gibbs sampler for convolutional networks, we need to sample from the conditional distribution of variables involved in convolutional layers and pooling layers.

1. Convolutional Layer

In this appendix we formulate the Gibbs sampler in the case of convolutional layers. The difficulty in this case stems from the structure in the weights. In this section we use the following notation

- C_ℓ is the number of channels in layer ℓ

- $H_W^{(\ell)}, W_W^{(\ell)}$ is the height and width of the convolutional filter $W^{(\ell)}$.
- $H_X^{(\ell)}, W_X^{(\ell)}$ are the height and width of the input $X^{(\ell)}$.
- $H_Z^{(\ell+1)}, W_X^{(\ell+1)}$ are the height and width of the output $Z^{(\ell+1)}$.
- K_ℓ is the size (i.e. $K_\ell = H_W^{(\ell)} \times W_W^{(\ell)}$) of each channel of filter $W^{(\ell)}$.
- d_ℓ , is the sizes of each channel in layer ℓ (i.e., the total number of variables at layer ℓ is $C_\ell \times d_\ell$)
- $\alpha, \alpha' \in [C_{\ell+1}]$ are the indices for the channel in layer $\ell + 1$
- $\beta, \beta' \in [C_\ell]$ are the indices for channels in layer ℓ .
- $a, a' \in [d_{\ell+1}]$ are indices for positions inside layer $\ell + 1$ (i.e. a specifies both the horizontal and vertical position within the layer)
- $b, b', c, c' \in [d_\ell]$ are indices for positions in layer ℓ .
- $r, r' \in [K_\ell]$ are indices for the position within the filter (e.g. if the filter is 3×3 then $K = 9$ and r runs over all the components of the filter)
- $i = (\beta, r)$ and $i' = (\beta', r')$ are used to group pairs of indices.

Commas will be used to separate indices, whenever there is ambiguity. The basic building block is the noisy convolutional layer, which has the following expression

$$Z_{\alpha a}^{(\ell+1)\mu} = \sum_{\beta=1}^{C_\ell} \sum_{r=1}^{K_\ell} W_{\alpha\beta r}^{(\ell)} X_{\beta, \nu_a(r)}^{(\ell)\mu} + (\epsilon_Z^{(\ell+1)})_{\alpha a}^\mu, \quad (\text{G1})$$

with $(\epsilon_Z^{(\ell+1)})_{\alpha a}^\mu \sim \mathcal{N}(0, \Delta_Z^{(\ell+1)})$. $W \in \mathbb{R}^{C_{\ell+1} \times C_\ell \times K_\ell}$. We also indicate with $\nu_a(r)$ the position of the r -th coordinate of the filter inside the input layer, when the output is in position a . In other words $\nu_a : [K_\ell] \mapsto [d_\ell]$. First we notice that $P(Z^{(\ell+1)} | W^{(\ell)}, X^{(\ell)}, X^{(\ell+1)})$ is basically unaffected by the structure of weights. We will concentrate on computing $P(W^{(\ell)} | Z^{(\ell+1)}, X^{(\ell)})$ and $P(X^{(\ell)} | Z^{(\ell+1)}, Z^{(\ell)}, W^{(\ell)})$. Let us begin by

$$P(W_\alpha^{(\ell)} | X^{(\ell)}, Z_\alpha^{(\ell+1)}) = \quad (\text{G2})$$

$$= \exp \left[-\frac{1}{2\Delta_Z^{(\ell+1)}} \sum_{a,\mu} \left(Z_{\alpha a}^{(\ell+1)\mu} - \sum_{\beta,r} W_{\alpha\beta r}^{(\ell)} X_{\beta, \nu_a(r)}^{(\ell)\mu} \right)^2 - \frac{\lambda_W^{(\ell)}}{2} \sum_{\beta,r} (W_{\alpha\beta r}^{(\ell)})^2 \right] = \quad (\text{G3})$$

$$= \exp \left[-\frac{1}{2} \sum_{\beta,r,\beta',r'} W_{\alpha\beta r}^{(\ell)} \left(\frac{1}{\Delta_Z^{(\ell+1)}} \sum_{\mu,a} X_{\beta, \nu_a(r)}^{(\ell)\mu} X_{\beta', \nu_a(r')}^{(\ell)\mu} + \lambda_W^{(\ell)} \delta_{rr'} \delta_{\beta\beta'} \right) W_{\alpha\beta' r'}^{(\ell)} \right] \quad (\text{G4})$$

$$+ \frac{1}{\Delta_Z^{(\ell+1)}} \sum_{\beta,r} W_{\alpha\beta r}^{(\ell)} \sum_{a,\mu} Z_{\alpha a}^{(\ell+1)\mu} X_{\beta, \nu_a(r)}^{(\ell)\mu} \Big] = \mathcal{N}(W_\alpha^{(\ell)} | (m_W^{(\ell)})_\alpha, \Sigma_W^{(\ell)}) \quad (\text{G5})$$

Computing these quantities requires grouping the two indices r, β into a single index and then inverting the matrix of the quadratic form in W . The double index matrix we would like to invert is

$$\tilde{A}_{\beta r, \beta' r'} = \frac{1}{\Delta_Z^{(\ell+1)}} \sum_{\mu,a} X_{\beta, \nu_a(r)}^{(\ell)\mu} X_{\beta', \nu_a(r')}^{(\ell)\mu} + \lambda_W^{(\ell)} \delta_{rr'} \delta_{\beta\beta'} \quad (\text{G6})$$

So we define $i = (\beta, r)$. Let $A_{ii'} = \tilde{A}_{\beta(i)r(i), \beta'(i')r'(i')} = A \left(\frac{1}{\Delta_Z^{(\ell+1)}} \sum_{\mu,a} X_{\beta(i), \nu_a(r(i))}^{(\ell)\mu} X_{\beta'(i'), \nu_a(r'(i'))}^{(\ell)\mu} + \lambda_W^{(\ell)} \delta_{r(i), r'(i')} \delta_{\beta(i), \beta'(i')} \right)$

then we define $\Sigma^{(W)} = A^{-1}$. Finally we define $\widetilde{A}^{-1}_{\beta r, \beta' r'} = A^{-1}_{i(\beta,r), i'(\beta',r')}$. In words, we're packing the indices of \tilde{A} , inverting it, and then unpacking the indices. For the mean we have

$$(m_W^{(\ell)})_{\alpha\beta r} = \frac{1}{\Delta_Z^{(\ell+1)}} \sum_{a,\mu} Z_{\alpha a}^{(\ell+1)\mu} \sum_{\beta', r'} [\widetilde{A}^{-1}]_{\beta r, \beta' r'} X_{\beta', \nu_a(r')}^{(\ell)\mu} \quad (\text{G7})$$

We now look at $P(X^{(\ell)}|Z^{(\ell+1)}, Z^{(\ell)}, W^{(\ell)})$. In the computation we use the identity $\sum_c \delta_{c, \nu_a(b)} = 1$

$$P(X^{(\ell)\mu}|Z^{(\ell+1)\mu}, Z^{(\ell)\mu}, W^{(\ell)}) = \quad (\text{G8})$$

$$= \exp \left[-\frac{1}{2\Delta_X^{(\ell)}} \sum_{\beta, b} \left(X_{\beta b}^{(\ell)\mu} - \sigma(Z_{\beta, b}^{(\ell)\mu}) \right)^2 - \frac{1}{2\Delta_Z^{(\ell+1)}} \sum_{a, \alpha} \left(Z_{\alpha a}^{(\ell+1)\mu} - \sum_{\beta, r} W_{\alpha\beta r}^{(\ell)} X_{\beta\nu_a(r)}^{(\ell)\mu} \right)^2 \right] \quad (\text{G9})$$

$$= \exp \left[-\frac{1}{2\Delta_X^{(\ell)}} \sum_{\beta, b} \left(X_{\beta b}^{(\ell)\mu} - \sigma(Z_{\beta b}^{(\ell)\mu}) \right)^2 \right] \quad (\text{G10})$$

$$- \frac{1}{2\Delta_Z^{(\ell+1)}} \sum_{a, \alpha} \left(Z_{\alpha a}^{(\ell+1)\mu} - \sum_{\beta, r} W_{\alpha\beta r}^{(\ell)} \sum_c \delta_{c, \nu_a(r)} X_{\beta\nu_a(r)}^{(\ell)\mu} \right)^2 \Big] \propto \quad (\text{G11})$$

$$\exp \left[-\frac{1}{2} \sum_{c, \beta, c', \beta'} X_{\beta c}^{(\ell)\mu} \left(\frac{1}{\Delta_X^{(\ell)}} \delta_{cc'} \delta_{\beta\beta'} + \frac{1}{\Delta_Z^{(\ell+1)}} \sum_{r, r', a, \alpha} W_{\alpha\beta r}^{(\ell)} W_{\alpha\beta' r'}^{(\ell)} \delta_{c, \nu_a(r)} \delta_{c', \nu_a(r')} \right) X_{\beta' c'}^{(\ell)\mu} \right] \quad (\text{G12})$$

$$+ \sum_{c, \beta} X_{\beta c}^{(\ell)\mu} \left(\frac{1}{\Delta_Z^{(\ell+1)}} \sum_{a, \alpha, r} \delta_{c, \nu_a(r)} Z_{\alpha a}^{(\ell+1)\mu} W_{\alpha\beta r}^{(\ell)} + \frac{1}{\Delta_\ell^{(X)}} \sigma(Z_{\beta c}^{(\ell)\mu}) \right) \Big] = \quad (\text{G13})$$

$$= \mathcal{N}(X^{(\ell)\mu} | (m_X^{(\ell)})^\mu, \Sigma_X^{(\ell)}) \quad (\text{G14})$$

As in the previous case we let A be the matrix of the quadratic form, with

$$\tilde{A}_{\beta c \beta' c'} = \frac{1}{\Delta_X^{(\ell)}} \delta_{cc'} \delta_{\beta\beta'} + \frac{1}{\Delta_Z^{(\ell+1)}} \sum_{r, r', a, \alpha} W_{\alpha\beta r}^{(\ell)} W_{\alpha\beta' r'}^{(\ell)} \delta_{c, \nu_a(r)} \delta_{c', \nu_a(r')} = \quad (\text{G15})$$

$$\frac{1}{\Delta_X^{(\ell)}} \delta_{cc'} \delta_{\beta\beta'} + \frac{1}{\Delta_Z^{(\ell+1)}} \sum_{\alpha} \sum_{c, c' \in \nu_a([K_\ell])} \sum_{r, r'} W_{\alpha\beta, \nu_a^{-1}(r)}^{(\ell)} W_{\alpha\beta', \nu_a^{-1}(r')}^{(\ell)} \quad (\text{G16})$$

In the last passage $\nu_a([K_\ell])$ indicates the image of the whole filter through ν_a . We basically incorporated the constraint that a should be such that c, c' are in the same subset of the input (if such as exist at all). As we did previously for W we group the indices using $i = (\beta, c)$ and $i' = (\beta', c')$. We then define the matrix $A_{ii'} = \tilde{A}_{\beta(i)c(i)\beta'(i')c'(i')}$, giving $\Sigma_X^{(\ell)} = A^{-1}$. For the mean we have

$$(m_X^{(\ell)})_{\beta c}^\mu = \sum_{c', \beta'} [\widetilde{A^{-1}}]_{\beta c \beta' c'} \left(\frac{1}{\Delta_Z^{(\ell+1)}} \sum_{a, \alpha, r} \delta_{c', \nu_a(r)} Z_{\alpha a}^{(\ell+1)\mu} W_{\alpha\beta' r}^{(\ell)} + \frac{1}{\Delta_\ell^{(X)}} \sigma(Z_{\beta' c'}^{(\ell)\mu}) \right) = \quad (\text{G17})$$

$$= \frac{1}{\Delta_X^{(\ell)}} \sum_{c', \beta'} [\widetilde{A^{-1}}]_{\beta c \beta' c'} \sigma(Z_{\beta' c'}^{(\ell)\mu}) + \frac{1}{\Delta_Z^{(\ell+1)}} \sum_{a, \alpha, r, \beta'} [\widetilde{A^{-1}}]_{\beta c \beta' \nu_a(r)} Z_{\alpha a}^{(\ell+1)\mu} W_{\alpha\beta' r}^{(\ell)} \quad (\text{G18})$$

2. Practical implementation

So far we packed the spatial (i.e. x and y coordinate within an image) in a single index. This allowed for more agile computations. We now unpack the indices and translate the results we obtained. In a practical case $X^{(\ell)} \in \mathbb{R}^{n \times C_\ell \times H_X^{(\ell)} \times W_X^{(\ell)}}$. For the weights we have $W^{(\ell)} \in \mathbb{R}^{C_{\ell+1} \times C_\ell \times H_W^{(\ell)} \times W_W^{(\ell)}}$. Let s_y, s_x be respectively the strides along the y, x axes. We do not use any padding. Then the height and width of $Z^{(\ell+1)}$ will be respectively $H_Z^{(\ell+1)} = \lfloor \frac{H_X^{(\ell)} - H_W^{(\ell)}}{s_y} \rfloor + 1$ and $W_Z^{(\ell+1)} = \lfloor \frac{W_X^{(\ell)} - W_W^{(\ell)}}{s_x} \rfloor + 1$.

Given $a = (a_y, a_x)$ the position inside layer $\ell + 1$ one can write $\nu_a(r) = \nu_a(r_y, r_x) = (r_y + s_y a_y, r_x + s_x a_x)$, yielding the following expression for the forward pass:

$$Z_{\alpha a_y a_x}^{(\ell+1)\mu} = \sum_{\beta=0}^{C_\ell-1} \sum_{r_x=0}^{W_W^{(\ell)}-1} \sum_{r_y=0}^{H_W^{(\ell)}-1} W_{\alpha\beta r_y r_x}^{(\ell)} X_{\beta, r_y + s_y a_y, r_x + s_x a_x}^{(\ell)\mu} + \epsilon^{(Z^{(\ell+1)})} \quad (\text{G19})$$

In ϵ we removed all the indices, for notation simplicity.

Recall we hat to compute the matrix \tilde{A} when sampling W . In this notation the expression for $\tilde{A} \in \mathbb{R}^{C_\ell \times H_W^{(\ell)} \times W_W^{(\ell)} \times C_\ell \times H_W^{(\ell)} \times W_W^{(\ell)}}$ becomes

$$\tilde{A}_{\beta r_y r_x \beta' r'_y r'_x} = \frac{1}{\Delta_Z^{(\ell+1)}} \sum_{\mu=0}^{n-1} \sum_{a_y=0}^{H_Z^{(\ell+1)}-1} \sum_{a_x=0}^{W_Z^{(\ell+1)}-1} X_{\beta, r_y + s_y a_y, r_x + s_x a_x}^{(\ell)\mu} X_{\beta', r'_y + s_y a_y, r'_x + s_x a_x}^{(\ell)\mu} + \quad (\text{G20})$$

$$+ \lambda_W^{(\ell)} \delta_{r_y, r'_y} \delta_{r_x, r'_x} \delta_{\beta, \beta'} \quad (\text{G21})$$

The expression for m_W in turn becomes

$$(m_W^{(\ell)})_{\alpha \beta r_y r_x} = \quad (\text{G22})$$

$$\frac{1}{\Delta_Z^{(\ell+1)}} \sum_{\mu=0}^{n-1} \sum_{a_y=0}^{H_Z^{(\ell+1)}-1} \sum_{a_x=0}^{W_Z^{(\ell+1)}-1} Z_{\alpha a_y a_x}^{(\ell+1)\mu} \sum_{\beta'=0}^{C_\ell-1} \sum_{r'_y=0}^{H_W^{(\ell)}-1} \sum_{r'_x=0}^{W_W^{(\ell)}-1} [\tilde{A}^{-1}]_{\beta r_y r_x, \beta' r'_y r'_x} X_{\beta', r'_y + s_y a_y, r'_x + s_x a_x}^{(\ell)\mu} \quad (\text{G23})$$

We now move to sampling $X^{(\ell)\mu}$. In that case we have

$$\tilde{A}_{\beta c \beta' c'} = \frac{1}{\Delta_X^{(\ell)}} \delta_{c c'} \delta_{\beta \beta'} + \frac{1}{\Delta_Z^{(\ell+1)}} \sum_{r, r', a, \alpha} W_{\alpha \beta r}^{(\ell)} W_{\alpha \beta' r'}^{(\ell)} \delta_{c, \nu_\alpha(r)} \delta_{c', \nu_\alpha(r')} \quad (\text{G24})$$

$$\tilde{A}_{\beta c_y c_x \beta' c'_y c'_x} = \frac{1}{\Delta_X^{(\ell)}} \delta_{c_y c'_y} \delta_{c_x c'_x} \delta_{\beta \beta'} + \quad (\text{G25})$$

$$+ \frac{1}{\Delta_Z^{(\ell+1)}} \sum_{r_y, r_x, r'_y, r'_x, a_y, a_x, \alpha} W_{\alpha \beta r_y r_x}^{(\ell)} W_{\alpha \beta' r'_y r'_x}^{(\ell)} \delta_{c_y, r_y + s_y a_y} \delta_{c_x, r_x + s_x a_x} \delta_{c'_y, r'_y + s_y a_y} \delta_{c'_x, r'_x + s_x a_x} \quad (\text{G26})$$

For $m_X^{(\ell)}$ we have

$$(m_X^{(\ell)})_{\beta c_x c_y} = \frac{1}{\Delta_X^{(\ell)}} \sum_{\beta', c'_y, c'_x} [\tilde{A}^{-1}]_{\beta c_y c_x \beta' c'_y c'_x} \sigma(Z_{\beta' c'_y c'_x}^{(\ell)\mu}) + \quad (\text{G27})$$

$$+ \frac{1}{\Delta_Z^{(\ell+1)}} \sum_{\alpha, a_y, a_x, r_y, r_x, \beta'} [\tilde{A}^{-1}]_{\beta c_y c_x \beta', r_y + s_y a_y, r_x + s_x a_x} Z_{\alpha a_y a_x}^{(\ell+1)\mu} W_{\alpha \beta' r_y r_x}^{(\ell)} \quad (\text{G28})$$

One can see that when the filter $W^{(\ell)}$ has dimensions (height and width) that are much smaller than those of $X^{(\ell)}$, then \tilde{A} will have few nonzero elements. In fact for $\tilde{A}_{\beta c_y c_x \beta' c'_y c'_x}$ to be nonzero, one must have that c, c' are close enough to be contained in the filter W . This implies that all the pairs of pixels c, c' with $|c_x - c'_x| > W_W^{(\ell)}$ or $|c_y - c'_y| > H_W^{(\ell)}$ will have $\tilde{A}_{\beta c_y c_x \beta' c'_y c'_x} = 0$. Hence \tilde{A} will be a sparse tensor. The same will somewhat be true in the covariance, which is the inverse of \tilde{A} .

3. Average Pooling

Here we look at how to put pooling into the mix. We focus on average pooling, which is easier since it is a linear transformation. For each pixel $b \in [d_\ell]$, let $P_\ell(b)$ ² be the "pooled pixel" in layer $\ell + 1$ to which b gets mapped. Hence we have $P : [d_\ell] \mapsto [d_{\ell+1}]$, a surjective function. Given a pixel a in layer $\ell + 1$ this will have multiple preimages through P , we denote the set of preimages as $P^{-1}(a)$. $P^{-1}(a)$ can therefore be seen as the receptive field of pixel a . Let

$$X_{\beta a}^{(\ell+1)\mu} = \frac{1}{|P^{-1}(a)|} \sum_{b \in P^{-1}(a)} X_{\beta b}^{(\ell)\mu} + (\epsilon_X^{(\ell+1)})_{\beta a}^\mu \quad (\text{G29})$$

² notice that for shape mismatch issues, some pixels could be mapped into nothing, so P only acts on the pixels that get pooled

be the generative model for the pooling layer. Notice we inject some noise $(\epsilon_X^{(\ell+1)})_{\beta a}^\mu \sim \mathcal{N}(0, \Delta_X^{(\ell+1)})$ in the output. The probability of $X^{(\ell)}$ factorizes according to the pooling receptive fields, i.e., pixels in different receptive fields are independent. Suppose also that we have $X_{\beta b}^{(\ell)\mu} = \sigma(X_{\beta b}^{(\ell-1)\mu}) + (\epsilon_X^{(\ell)})_{\beta b}^\mu$, with $(\epsilon_X^{(\ell)})_{\beta b}^\mu \sim \mathcal{N}(0, \Delta_X^{(\ell)})$. $\sigma(\cdot)$ here can be an element wise activation function, but it can also represent any other transformation³. We have

$$P(\{X_{\beta,b}^{(\ell)\mu}\}_{b \in P^{-1}(a)} | \{X_{\beta,b}^{(\ell-1)\mu}\}_{b \in P^{-1}(a)}, X_{\beta,a}^{(\ell+1)\mu}) = P(X_{\beta,a}^{(\ell+1)\mu} | \{X_{\beta,b}^{(\ell)\mu}\}_{b \in P^{-1}(a)}) \times \quad (\text{G30})$$

$$\times \prod_{b \in P^{-1}(a)} P(X_{\beta b}^{(\ell)\mu} | X_{\beta b}^{(\ell-1)\mu}) \propto \exp \left[-\frac{1}{2\Delta_X^{(\ell)}} \sum_{b \in P^{-1}(a)} \left(X_{\beta b}^{(\ell)\mu} - \sigma(X_{\beta b}^{(\ell-1)\mu}) \right)^2 \right] \quad (\text{G31})$$

$$- \frac{1}{2\Delta_X^{(\ell+1)}} \left(X_{\beta a}^{(\ell+1)\mu} - \frac{1}{|P^{-1}(a)|} \sum_{b \in P^{-1}(a)} X_{\beta b}^{(\ell)\mu} \right)^2 \Big] \propto \quad (\text{G32})$$

$$\exp \left[-\frac{1}{2} \sum_{b,c \in P^{-1}(a)} X_{\beta b}^{(\ell)\mu} \left(\frac{1}{\Delta_X^{(\ell)}} \delta_{bc} + \frac{1}{\Delta_X^{(\ell+1)} |P^{-1}(a)|^2} \right) X_{\beta c}^{(\ell)\mu} + \right] \quad (\text{G33})$$

$$+ \sum_{b \in P^{-1}(a)} X_{\beta b}^{(\ell)\mu} \left(\frac{\sigma(X_{\beta b}^{(\ell-1)\mu})}{\Delta_X^{(\ell)}} + \frac{X_{\beta a}^{(\ell+1)\mu}}{\Delta_X^{(\ell+1)} |P^{-1}(a)|} \right) \Big] \propto \mathcal{N}(\{X_{\beta,b}^{(\ell)\mu}\}_{b \in P^{-1}(a)} | m_X^{(\ell)}_\beta, \Sigma_X^{(\ell)}) \quad (\text{G34})$$

With $\Sigma_X^{(\ell)} \in \mathbb{R}^{P^{-1}(a) \times P^{-1}(a)^4}$ as $\Sigma_X^{(\ell)} = \left(\frac{1}{\Delta_X^{(\ell)}} \mathbb{1} + \frac{1}{\Delta_X^{(\ell+1)} |P^{-1}(a)|^2} \mathbf{1}\mathbf{1}^T \right)^{-1}$ and $(m_X^{(\ell)})_{\beta b}^\mu = \sum_b (\Sigma_X^{(\ell)})_{bc} \left(\frac{\sigma(X_{\beta c}^{(\ell-1)\mu})}{\Delta_X^{(\ell)}} + \frac{X_{\beta a}^{(\ell+1)\mu}}{\Delta_X^{(\ell+1)} |P^{-1}(a)|} \right)$

Exploiting the fact that $\Sigma_X^{(\ell)}$ is a projector plus the identity one can simplify the previous expressions. We use the fact that for a matrix $A = r\mathbb{1} + svv^T$, with $r, s \in \mathbb{R}$, $v \in \mathbb{R}^n$, its inverse is $A^{-1} = \frac{1}{r}\mathbb{1} - \frac{s}{r^2 + rs\|v\|^2} vv^T$. In our present case $r = 1/\Delta_X^{(\ell)}$, $s = \frac{1}{\Delta_X^{(\ell+1)} |P^{-1}(a)|^2}$ and $v = \mathbf{1}$, $v \in \mathbb{R}^{|P^{-1}(a)|}$. This gives (keeping implicit that $a = P(b)$),

$$(m_X^{(\ell)})_{\beta b}^\mu = \sigma(X_{\beta b}^{(\ell-1)\mu}) + \frac{\Delta_X^{(\ell)}}{\Delta_X^{(\ell)} + |P^{-1}(a)|\Delta_X^{(\ell+1)}} \left(X_{\beta a}^{(\ell+1)\mu} - \frac{1}{|P^{-1}(a)|} \sum_{c \in P^{-1}(a)} \sigma(X_{\beta c}^{(\ell-1)\mu}) \right) \quad (\text{G35})$$

$$\begin{aligned} \Sigma_X^{(\ell)} &= \mathbb{E} \left[X_\beta^{(\ell)\mu} (X_\beta^{(\ell)\mu})^T \right] - (m_X^{(\ell)})_\beta^\mu (m_X^{(\ell)})_\beta^{\mu T} = \\ &= \Delta_X^{(\ell)} \mathbb{1} - \frac{(\Delta_X^{(\ell)})^2}{|P^{-1}(a)|(|P^{-1}(a)|\Delta_X^{(\ell+1)} + \Delta_X^{(\ell)})} \mathbf{1}\mathbf{1}^T \end{aligned} \quad (\text{G36})$$

To generate a Gaussian variable with this covariance we employ the following trick. Suppose $\Sigma = r\mathbb{1}_d - svv^T$ (i.e., identity minus a projector) and $z \sim \mathcal{N}(0, r\mathbb{1}_d)$. Define $\bar{z} = z - q\langle z, v \rangle$, with $q = \frac{1}{\|v\|^2} \left(1 - \sqrt{1 - \frac{s\|v\|^2}{r}} \right)$. Then $\bar{z} \sim \mathcal{N}(0, \Sigma)$. In our case, we have $v = \mathbf{1}$, $r = \Delta_X^{(\ell)}$, $s = \frac{(\Delta_X^{(\ell)})^2}{|P^{-1}(a)|(|P^{-1}(a)|\Delta_X^{(\ell+1)} + \Delta_X^{(\ell)})}$. This gives $q = \frac{1}{|P^{-1}(a)|} \left(1 - \sqrt{\frac{|P^{-1}(a)|\Delta_X^{(\ell+1)}}{|P^{-1}(a)|\Delta_X^{(\ell+1)} + \Delta_X^{(\ell)}}$

It can happen that the pooling layer size is not perfectly matched to the image size (i.e., $H_X^{(\ell)}/H_W^{(\ell)}$ is not an integer). In this case, we define $H_X^{(\ell+1)} = \lfloor H_X^{(\ell)}/H_W^{(\ell)} \rfloor$ (basically we discard the last part of the input layer). The pixels that do not contribute to $X^{(\ell+1)}$ should be sampled from $\mathcal{N}(\sigma(X_{\beta b}^{(\ell-1)\mu}), \Delta_X^{(\ell)})$.

Sampling $X^{(\ell+1)}$ does not require any additional custom function. In fact $P(X^{(\ell+1)} | W^{(\ell+1)}, X^{(\ell+2)}, X^{(\ell)})$ is equal to (G8), where $\Delta_X^{(\ell)} \mapsto \Delta_X^{(\ell+1)}$, $\Delta_Z^{(\ell+1)} \mapsto \Delta_{\ell+2}^{(X)}$, and the nonlinearity σ is replaced by the pooling layer expression.

³ for example the same scheme can be used to have a convolutional layer followed by a pooling layer. Just set $\sigma(x) = x$ and $X^{(\ell)} = \text{Conv2d}(W^{(\ell-2)}, X^{(\ell-2)})$ (notice the absence of noise). Here Conv2d executes the 2d convolution between its inputs.

⁴ In principle the size depends on a , however normally each pixel in layer $\ell + 1$ has the same number of preimages.

4. Biases

In the convolutional networks the biases are introduced by writing the layer as

$$Z_{\alpha a}^{(\ell+1)\mu} = \sum_{\beta=1}^{C_\ell} \sum_{r=1}^{K_\ell} W_{\alpha\beta r}^{(\ell)} X_{\beta\nu_a(r)}^{(\ell)\mu} + b_\alpha^{(\ell)} + (\epsilon_Z^{(\ell+1)})_{\alpha a}^\mu, \quad (\text{G37})$$

where $b_\alpha^{(\ell)} \sim \mathcal{N}(0, 1/\lambda_b^{(\ell)})$, and $(\epsilon_Z^{(\ell+1)})_{\alpha a}^\mu \sim \mathcal{N}(0, \Delta_Z^{(\ell+1)})$. Notice that there is one bias parameter per channel. Sampling $W^{(\ell)}, X^{(\ell)}$ is very similar to the previous case. One must simply replace $Z_{\alpha a}^{(\ell+1)\mu} \mapsto Z_{\alpha a}^{(\ell+1)\mu} - b_\alpha^{(\ell)}$. When sampling $Z_{\alpha a}^{(\ell+1)\mu}$ instead one should instead replace $\sum_{\beta r} W_{\alpha\beta r}^{(\ell)} X_{\beta\nu_a(r)}^{(\ell)\mu} \mapsto \sum_{\beta r} W_{\alpha\beta r}^{(\ell)} X_{\beta\nu_a(r)}^{(\ell)\mu} - b_\alpha^{(\ell)}$.

The update equation for the biases is

$$P(b_\alpha^{(\ell)} | Z_\alpha^{(\ell+1)}, X^{(\ell)}, W^{(\ell)}) \propto P(Z_\alpha^{(\ell+1)} | b_\alpha^{(\ell)}, X^{(\ell)}, W^{(\ell)}) P(b_\alpha^{(\ell)} | X^{(\ell)}, W^{(\ell)}) = \quad (\text{G38})$$

$$= P(Z_\alpha^{(\ell+1)} | b_\alpha^{(\ell)}, X^{(\ell)}, W^{(\ell)}) P(b_\alpha^{(\ell)}) \propto \quad (\text{G39})$$

$$\propto \exp \left[-\frac{1}{2} \left(\frac{nd_{\ell+1}}{\Delta_Z^{(\ell+1)}} + \lambda_b^{(\ell)} \right) (b_\alpha^{(\ell)})^2 + \frac{1}{\Delta_Z^{(\ell+1)}} \sum_{\mu a} \left(Z_{\alpha a}^{(\ell+1)\mu} - \sum_{\beta r} W_{\alpha\beta r}^{(\ell)} X_{\beta\nu_a(r)}^{(\ell)\mu} \right) \right] = \quad (\text{G40})$$

$$= \mathcal{N} \left(b_\alpha^{(\ell)} \left| \frac{\sum_{\mu a} \left(Z_{\alpha a}^{(\ell+1)\mu} - \sum_{\beta r} W_{\alpha\beta r}^{(\ell)} X_{\beta\nu_a(r)}^{(\ell)\mu} \right)}{nd_{\ell+1} + \Delta_Z^{(\ell+1)} \lambda_b^{(\ell)}}, \frac{\Delta_Z^{(\ell+1)}}{nd_{\ell+1} + \lambda_b^{(\ell)} \Delta_Z^{(\ell+1)}} \right. \right) \quad (\text{G41})$$

Appendix H: Other Monte Carlo algorithms

In this appendix, we provide the pseudocode for HMC on the classical posterior, HMC on the intermediate noise posterior and MALA on the classical posterior

1. Hamiltonian Monte Carlo

We provide the pseudocode of HMC (algorithm 3). In the paper we used the implementation from [11] for synthetic data and the one in [8] for real-world data. The algorithm depends on the learning rate and the number of leapfrog steps, which are hyperparameters that need to be optimized appropriately.

Algorithm 3 Hamiltonian Monte Carlo

Input: Probability measure to sample $\pi(x)$, initial condition x_0 , step size η , number of leapfrog steps L , length of the simulation t_{\max} .

Output: a sequence S of samples

$S \leftarrow [x_0]$

for $i = 1$ to t_{\max} **do**

$p \sim \mathcal{N}(0, \mathbb{1})$

 ▷ Sample a new momentum from a normal distribution

$x \leftarrow x_0$

$\mathcal{H} \leftarrow \pi(x_0) - \frac{\|p\|^2}{2}$

for $j = 1$ to L **do**

 ▷ Simulate Hamiltonian dynamics to propose a new state

$p \leftarrow p - \frac{\epsilon}{2} \nabla \pi(x)$

 ▷ Simulate a half-step for momentum

$x \leftarrow x + \epsilon p$

 ▷ Simulate a full-step for position

$p \leftarrow p - \frac{\epsilon}{2} \nabla \pi(x)$

 ▷ Simulate another half-step for momentum

end for

$\mathcal{H}_{\text{prop}} \leftarrow \pi(x) - \frac{\|p\|^2}{2}$

 ▷ Compute the proposed Hamiltonian

$z \sim \text{Uniform}([0, 1])$

if $\log(z) < \mathcal{H} - \mathcal{H}_{\text{prop}}$ **then**

 ▷ Accept/Reject the proposal

$x_0 \leftarrow x$

end if

$S.append(x_0)$

end for

2. Metropolis Adjusted Langevin Algorithm

The pseudocode for MALA is reported here (algorithm 4). In the paper we used the implementation in [11] for synthetic data and a custom implementation for real data. The algorithm has on one hyper-parameter: the learning rate. If the learning rate is too large the Metropolis acceptance rate gets too low. Lowering the learning rate increases the acceptance rate up to an optimal value, after which the acceptance rate starts decreasing again.

Algorithm 4 Metropolis Adjusted Langevin Algorithm (MALA)

Input: Probability measure to sample $\pi(\cdot)$, initial condition x , step size η , length of the simulation t_{\max} .
Output: a sequence S of samples
 $S \leftarrow [x]$
for $t = 1, \dots, t_{\max}$ **do**
 $x' \leftarrow x + \eta \nabla \pi(x) + \sqrt{2\eta} \mathcal{N}(0, 1)$ ▷ The Gaussian noise is i.i.d. over the coordinates of W
 $P_{x \rightarrow x'} \leftarrow \exp \left[-\frac{1}{4\eta} (x' - x - \eta \nabla \pi(x))^2 \right]$
 $P_{x' \rightarrow x} \leftarrow \exp \left[-\frac{1}{4\eta} (x - x' - \eta \nabla \pi(x'))^2 \right]$
 $P_{\text{acc}} \leftarrow \min \left\{ 1, \frac{\pi(x') P_{x' \rightarrow x}}{\pi(x) P_{x \rightarrow x'}} \right\}$ ▷ Acceptance probability according to Metropolis rule
 $z \sim \text{Uniform}([0, 1])$
if $z < P_{\text{acc}}$ **then** ▷ If accepted update x
 $x' \leftarrow x$
end if
 $S.\text{append}(x)$
end for

Appendix I: Synthetic data experiments

This appendix provides additional details about the numerical experiments on synthetic data presented in section V B. We recall that in these experiments we ran Gibbs on the intermediate noise posterior, MALA on the classical posterior and HMC both on the intermediate and classical posterior. For MALA and HMCs we used the implementation contained in [11]. To produce the left plot in figure 2, we ran each algorithm with 3 logarithmically spaced values of Δ per decade, both from the informed and uninformed initialization. For each value of Δ and each initialization we further ran each algorithm 72 times, each time with different teacher network, random student initialization (whenever this initialization was used) and noise in the MCMC. For the Gibbs sampler we set all variables to zero in the uninformed initialization. Instead for the HMCs and MALA, still in the uninformed case, we found that initializing the variables as i.i.d. Gaussians with standard deviation 10^{-4} helped the algorithms thermalize. We remark that not having to tune the initialization norm, is another advantage of the Gibbs sampler.

The HMCs and MALA all have hyperparameters to select. The optimal parameters were obtained by doing a grid search on the learning rate and, in the case of HMC, number of leapfrog steps. For each value of Δ we re-optimize the hyperparameters. In the case of HMC, we build our grid by trying 3 learning rates per decade and two numbers of leapfrog steps per decade. In the case of MALA we try three learning rates per decade. For both MALA and HMC we select the hyperparameters for which the test MSE takes the least time to descend and subsequently become stationary. The optimal values of the hyper parameters, as well as the number of steps in each simulation, are in tables II, I for HMC and tables III, IV for MALA. For Gibbs all experiments were run for 2.5×10^6 steps. The number of steps of the different algorithms has been chosen so that the runs executed within 5:30h. All experiments were run on one core of Intel Xeon Platinum 8360Y running at 2.4 GHz.

Appendix J: Real data experiments

In this appendix, we provide the details of the experiments conducted in sections V B. We start by describing the architectures used. In the case of the MLP with 12 hidden units, the model is

$$f_{\text{MLP}}(x, W) = \arg \max_{\alpha} \left[W_{\alpha}^{(2)T} \sigma(W^{(1)}x + b^{(1)}) + b_{\alpha}^{(2)} \right], \quad (\text{J1})$$

with $x \in \mathbb{R}^{784}$, $W^{(1)} \in \mathbb{R}^{12 \times 784}$, $b^{(1)} \in \mathbb{R}^{12}$, $W^{(2)} \in \mathbb{R}^{10 \times 12}$, $b^{(2)} \in \mathbb{R}^{10}$ and $\sigma(x) = \max(0, x)$. α is the row index of $W^{(2)}$. To apply the Gibbs sampler we must translate this architecture into a posterior using the intermediate noise

TABLE I. Parameters for HMC with intermediate noise posterior on syntetic data. HMC Steps is the total number of Metropolis steps during the run. For the plots in Figure 2 a measurement is taken every 10 steps.

Delta	Learning Rate	Leapfrog Steps	HMC Steps
1.0×10^0	5.0×10^{-4}	10^3	10^4
4.64×10^{-1}	5.0×10^{-4}	10^3	10^4
2.15×10^{-1}	5.0×10^{-4}	10^3	10^4
1.0×10^{-1}	5.0×10^{-4}	10^3	10^4
4.64×10^{-2}	5.0×10^{-4}	10^3	10^4
2.15×10^{-2}	5.0×10^{-4}	10^3	10^4
1.0×10^{-2}	5.0×10^{-4}	10^3	10^4
4.64×10^{-3}	5.0×10^{-5}	10^3	10^5
2.15×10^{-3}	5.0×10^{-5}	10^3	10^5
1.0×10^{-3}	5.0×10^{-5}	10^3	10^5
4.64×10^{-4}	5.0×10^{-5}	10^3	10^5
2.15×10^{-4}	5.0×10^{-5}	10^3	10^5
1.0×10^{-4}	5.0×10^{-5}	10^3	10^5
4.64×10^{-5}	5.0×10^{-5}	10^3	10^5
2.15×10^{-5}	5.0×10^{-5}	10^3	10^5
1.0×10^{-5}	5.0×10^{-5}	10^3	10^5

TABLE II. Parameters for HMC with classical posterior on syntetic data. HMC Steps is the total number of Metropolis steps during the run. For the plots in Figure 2 a measurement is taken every 10 steps.

Delta	Learning Rate	Leapfrog Steps	HMC Steps
1.0×10^0	5.0×10^{-4}	2.0×10^1	10^4
4.64×10^{-1}	5.0×10^{-4}	2.0×10^1	10^4
2.15×10^{-1}	5.0×10^{-4}	2.0×10^1	10^4
1.0×10^{-1}	5.0×10^{-4}	2.0×10^1	10^4
4.64×10^{-2}	5.0×10^{-4}	2.0×10^1	10^4
2.15×10^{-2}	5.0×10^{-5}	10^2	10^5
1.0×10^{-2}	5.0×10^{-5}	10^2	10^5
4.64×10^{-3}	5.0×10^{-5}	10^3	10^5
2.15×10^{-3}	5.0×10^{-5}	10^3	10^5
1.0×10^{-3}	5.0×10^{-5}	10^3	10^5
4.64×10^{-4}	5.0×10^{-5}	10^3	10^5
2.15×10^{-4}	5.0×10^{-5}	10^3	10^5
1.0×10^{-4}	5.0×10^{-5}	10^3	10^5

TABLE III. Parameters for MALA on synthetic data with informed initialisation. Langevin Steps is the number of steps during each run. Measurements of the test MSE, as reported in Figure 2 are taken every *Spacing* steps.

Delta	Learning Rate	Langevin Steps	Spacing
1.0×10^0	1.0×10^{-5}	10^5	10^2
4.64×10^{-1}	1.0×10^{-5}	10^5	10^2
2.15×10^{-1}	1.0×10^{-5}	10^5	10^2
1.0×10^{-1}	1.0×10^{-5}	10^5	10^2
4.64×10^{-2}	1.0×10^{-5}	10^6	10^2
2.15×10^{-2}	1.0×10^{-6}	10^6	10^2
1.0×10^{-2}	1.0×10^{-6}	10^6	10^2
4.64×10^{-3}	1.0×10^{-6}	10^6	10^2
2.15×10^{-3}	1.0×10^{-6}	10^6	10^2
1.0×10^{-3}	1.0×10^{-6}	10^6	10^2
4.64×10^{-3}	1.0×10^{-7}	10^6	10^2
2.15×10^{-3}	1.0×10^{-7}	10^6	10^2
1.0×10^{-4}	1.0×10^{-7}	10^6	10^2
4.64×10^{-4}	1.0×10^{-9}	1.1×10^7	1.1×10^3
2.15×10^{-4}	1.0×10^{-9}	1.1×10^7	1.1×10^3
1.0×10^{-5}	1.0×10^{-9}	1.1×10^7	1.1×10^3

TABLE IV. Parameters for MALA on synthetic data with zero initialisation. Langevin Steps is the number of steps during each run. Measurements of the test MSE, as reported in Figure 2 are taken every *Spacing* steps.

Delta	Learning Rate	Langevin Steps	Spacing
1.0×10^0	1.0×10^{-5}	10^5	10^2
4.64×10^{-1}	1.0×10^{-5}	10^5	10^2
2.15×10^{-1}	1.0×10^{-5}	10^6	10^2
1.0×10^{-1}	1.0×10^{-5}	10^6	10^2
4.64×10^{-2}	1.0×10^{-5}	10^6	10^2
2.15×10^{-2}	1.0×10^{-6}	10^6	10^2
1.0×10^{-2}	1.0×10^{-7}	1.1×10^7	1.1×10^3
4.64×10^{-3}	1.0×10^{-7}	1.1×10^7	1.1×10^3
2.15×10^{-3}	1.0×10^{-7}	1.1×10^7	1.1×10^3
1.0×10^{-3}	1.0×10^{-8}	1.1×10^7	1.1×10^3
4.64×10^{-3}	1.0×10^{-8}	1.1×10^7	1.1×10^3
2.15×10^{-3}	1.0×10^{-9}	1.1×10^7	1.1×10^3
1.0×10^{-4}	1.0×10^{-9}	1.1×10^7	1.1×10^3
4.64×10^{-4}	1.0×10^{-10}	1.1×10^7	1.1×10^3
2.15×10^{-4}	1.0×10^{-10}	1.1×10^7	1.1×10^3
1.0×10^{-5}	1.0×10^{-11}	1.1×10^7	1.1×10^3
4.64×10^{-6}	1.0×10^{-11}	1.1×10^7	1.1×10^3

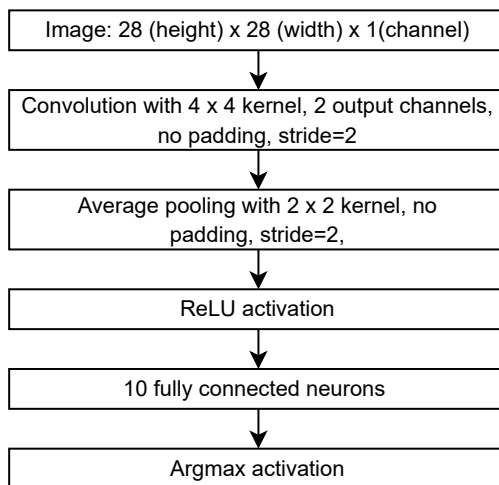


FIG. 5. CNN architecture used in the experiments of section VB. The convolutional layer is composed of the filter $W^{(1)}$ with shape $2 \times 1 \times 4 \times 4$ and a output channel bias $b^{(1)} \in \mathbb{R}^2$. The final layer instead has weights $W^{(2)} \in \mathbb{R}^{72 \times 10}$ and bias $b^{(2)} \in \mathbb{R}^{10}$.

model. To do so, the additional variables $Z^{(2)} \in \mathbb{R}^{n \times 12}$, $X^{(2)} \in \mathbb{R}^{n \times 12}$, $Z^{(3)} \in \mathbb{R}^{n \times 10}$ are introduced, with $n = 6 \times 10^4$ in the case of MNIST. A noise with variance Δ is put on $Z^{(2)}$, $X^{(2)}$. Notice there is no noise between $Z^{(3)}$ and the labels y . Hence the posterior has the hard constraint $y^\mu = \arg \max_{\alpha \in \{0,1,\dots,9\}} Z_\alpha^{(3)\mu}$. The priors on the parameters are given by: $\lambda_W^{(1)} = \lambda_b^{(1)} = 784$, $\lambda_W^{(2)} = \lambda_b^{(2)} = 12$. On the intermediate noise posterior we ran experiments with $\Delta = 2$, and all variables were set to zero at initial condition.

In the case of the classical posterior, we ran experiments with $\Delta = 2$ using MALA and HMC as algorithms. The value of Δ was picked so that the test error at stationarity is the same as in the intermediate noise posterior. The optimal parameters of HMC are a learning rate of 10^{-3} and 200 leapfrog steps, while for MALA the optimal learning rate is 2×10^{-6} . For HMC, MALA the variables were initialized as i.i.d. Gaussians with respective standard deviations 10^{-1} , 10^{-4} .

Regarding the CNN, we provide a schematic representation of the architecture in figure 5. In the intermediate noise model a noise is added after the convolution, after the average pooling, after the ReLU, and after the fully connected layer. All noises are i.i.d. Gaussians with variance Δ , as prescribed by the intermediate noise model. To complete the description, we specify the prior. We set $\lambda_W^{(1)} = \lambda_b^{(1)} = 16$, $\lambda_W^{(2)} = \lambda_b^{(2)} = 72$.

In the intermediate noise posterior, we run the Gibbs sampler with $\Delta = 100$, and initialize all variables to zero. For

the classical posterior, we run MALA and HMC on the CNN architecture, with $\Delta = 10$. This value of Δ leads to approximately the same test error as in the intermediate noise posterior. For HMC we use a learning rate of 10^{-3} and 50 leapfrog steps, while for MALA we choose 5×10^{-6} as learning rate.

Both for MLP and CNN, in the case of the classical posterior, we have to specify a loss function. To do so we replace the argmax in the last layer by a softmax and apply a cross entropy loss on top of the softmax. Calling $Q \in \mathbb{R}^{n \times 10}$ the output of the softmax, the loss function is $\ell(y^\mu, Q^\mu) = -\log Q_{y^\mu}^\mu$. The argmax is however still used when making predictions, for example when evaluating the model on the test set. All experiments were run on one NVIDIA V100 PCIe 32 GB GPU and one core of Xeon-Gold running at 2.1 GHz.